Modeling of Electrokinetic Mixing in Lab on Chip Microfluidic Devices

Majarikar Virendra Jiwanrao

A Dissertation Submitted to

Indian Institute of Technology Hyderabad

In Partial Fulfillment of the Requirements for

The Degree of Master of Technology

भारतीय प्रौद्योगिकी संस्थान हैदराबाद

Indian Institute of Technology Hyderabad

Department of Biomedical Engineering

July, 2016

Declaration

I declare that this written submission represents my ideas in my own words, and where others' ideas or words have been included, I have adequately cited and referenced the original sources. I also declare that I have adhered to all principles of academic honesty and integrity and have not misrepresented or fabricated or falsified any idea/data/fact/source in my submission. I understand that any violation of the above will be a cause for disciplinary action by the Institute and can also evoke penal action from the sources that have thus not been properly cited, or from whom proper permission has not been taken when needed.

V J Majaridal

_____

(Signature)

MAJARIKAR VIRENDRA JIWANRAO

_____

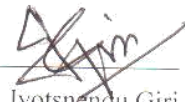(– Student Name –)

BM14MTECH11004

_____

(Roll No)

Approval Sheet

This thesis entitled "Modeling of Electrokinetic Mixing in Lab on Chip Microfluidic Devices" by Majarikar Virendra Jiwanrao is approved for the degree of Master of Technology from IIT Hyderabad.

Dr. Jyoti Ranjan Mohanty
Assistant Professor
Department of Physics
Indian Institute of Technology, Hyderabad
Examiner

Dr. Jyotsnendu Giri
Assistant Professor
Department of Biomedical Engineering
Indian Institute of Technology Hyderabad
Examiner

Dr. Harikrishnan N. Unni
Assistant Professor
Department of Biomedical Engineering
Indian Institute of Technology Hyderabad
Adviser

Acknowledgements

Abstract

This dissertation summarize a modeling of electrokinetic mixing employing electro-osmotic stationary and time-dependent micropumps via alternate zeta potential patches on the lower surface of the mixing chamber in lab on chip microfluidic device. Electro-osmotic flow is augmented using different model designs with alternate zeta potential values such as 25mV, 50mV and 100mV respectively to achieve high mixing efficiency in electrokinetically driven microfluidic system. The enhancement of mixing via alternate opposing zeta potentials is studied using Finite Element Modeling. Simulation 2D and 3D workflow involves designated steps such as setting up the model environment, creating geometric objects, stipulating materials and boundary conditions, meshing and post analyzing the results. An electric contours and concentration gradients are derived using a Navier-Stokes for incompressible flow, convection-diffusion equation and Helmholtz-Smoluchowski slip velocity respectively. The effect of magnitude of zeta potential, number of alternate patches etc. are studied in detail. In addition, 2D results are compared with 3D results to demonstrate the significance of 3D model in microfluidic design process.

Nomenclature

ζ	Zeta potential
c	Concentration
$\partial c/\partial t$	Concentration gradient
$\partial v/\partial t$	Unsteady acceleration
$(v.\nabla)v$	Convective acceleration
$-\nabla p$	Pressure gradient
u	Velocity
ε_w	Fluid's electric permittivity
V	Electric potential
η	Dynamic viscosity of the liquid
E	Electric field
f	External forces
ρ	Fluid density
D	Diffusion coefficient of the solution
R	Reaction rate

List of Figures

List of Tables

Contents

Chapter 1

Introduction

1.1   Electrokinetics

In presence of an electric field, electrokinetics represent the study of liquid or motion of particle [1]; in general, the phenomena relating to the direct alteration of electrical energy into kinetic energy, and vice versa. The applications of electrokinetics in advances of microfluidic devices have been appreciated worldwide and serves as a feasible tool in inventing a lab-on-a-chip for use in biological and chemical assays, manipulating fluids for several scientific and industrial contexts in the past decade.

The history of electrokinetics [2] can be traced back to the year 1808 where F. Reuss first observed the electrokinetic (EK) effect using DC applied to clay-water mixture. During the mid-nineteenth century, Napier discovered the distinction between electro-osmosis and electrophoresis. In the striking discovery, H. Helmholtz developed the analytical models for the electrokinetics in late 1879. A combination of work between Pellat (1904) and Smoluchowski (1921) derived the electrokinetic velocity using Helmholtz model extension. In the year 1941, L. Casagrande demonstrates electrokinetic phenomena in porous media like soil. Electrokinetics discovered continued with the early investigators including G. Wiedemann, G.Quincke, E. Dorn and many more.

The various electrokinetic technique covering the particle and fluid transport mechanisms: electroosmosis, dielectrophoresis, electrophoresis, electrowetting, electrokinetic instability, etc.

1.1.1 Electroosmosis

Under the influence of an applied electric field, electroosmosis constitute motion of a liquid through an immobilized particles, a porous mass, or a membrane. In other words, movement of electrolyte containing fluid relative to a stationary charged surface by an applied electric field [3-12]. It resulted into the moving ions dragging the liquid, in which they are embedded, due to the force exerted by the electric field on the counter-charge in the liquid inside the charged capillaries, pores, etc. Figure 1.1 shows the electroosmotic phenomena. The chemical equilibrium between an electrolyte and solid functional surfaces leads to the layer of mobile ions with net electrical charge near the interface, known as an electrical double layer. Electroosmotic flow is the outcome of the Coulomb force induced by an electric field on net mobile electric charge in the electrical double layer. The uniform velocity of the liquid far from the charged interface constitute the electroosmotic velocity (m/s). Usually, the measured quantity is the volume flow rate of liquid through the capillary, porous plug, or membrane.

Cross section

Inside capillary cut along lenght
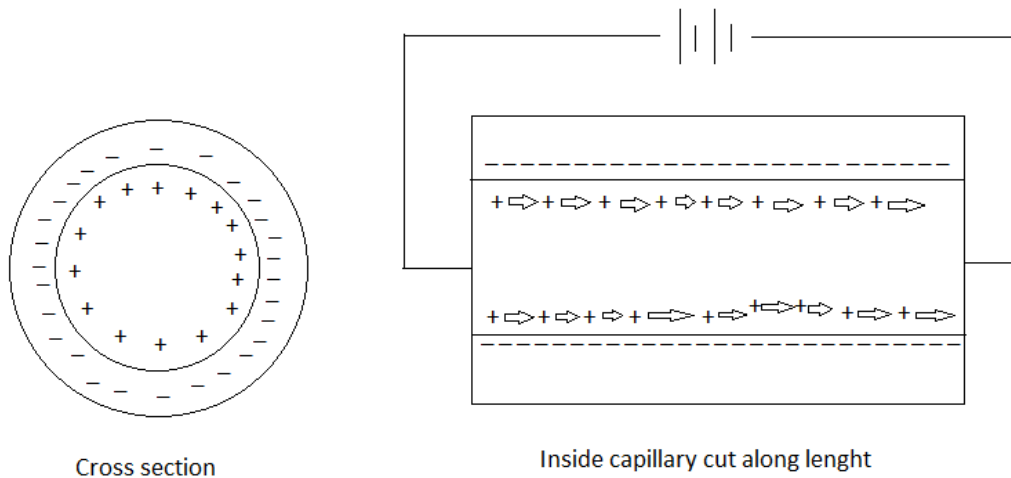
Figure 1.1 Sketch of the electroosmotic phenomena.
Diagram produced based on reference [3].

It is classified into two subfields:

Classical electroosmosis

It depend on surface charges from the surface functional groups attracting counter-ions from the electrolyte solution and repel con-ions maintaining local electroneutrality [1, 4].

Electrical double layer (EDL) formation by excess of charge near the solid-liquid interface with a thickness equal to the Debye screening length.

Field-induced electroosmosis

This electroosmosis involve formation of double layer polarization near the solid–liquid interface due to surface charges induced by the external electric field [1, 5]. Measurement of frequency-dependent fluid velocity is observed during the AC electrokinetic particle manipulation in suspension on solid–liquid interface. The fluid movement is a function of electrode position and frequency, and frequencies below the corresponding relaxation time of ions.

1.1.2   Electrical double layer

Electrical double layer occurs at the interface when an electrode is immersed into an electrolyte solution with variation of electric potential near an electrode surface, resulting the structure of charge accumulation and charge separation [13]. Accumulation of excess ions of the opposite charge in the solution, function of the electrode potential, being compensated by the excess charge on the electrode surface.

Electrical double layer compose of two parallel layers of charge surrounding the object which may be solid particle, liquid droplet or some porous materials. The initial layer, called stern layer, comprises ions, either positive or negative, adsorbed onto the object due to chemical interactions. The second layer, called diffuse layer, is loosely associated with the object and consist of free moving ions, both positive and negative, that move in the fluid under the influence of electric attraction towards surface charge via the Coulomb force, electrically shielding the stern layer.

1.1.3   Electrowetting

Electrowetting involve altering the surface tension of liquids using a voltage on a solid surface and commonly used technique for small amounts of liquids manipulation on surfaces [14]. It involve the application of reduction in contact angle and the entire droplets motion on to the solid surface owing to electrostatic forces. Saturation of the contact angle at high voltage, electric fields inducing liquid surface distortions, electric fields penetration depth range into the liquid, and in the presence of AC voltage, conductivity and electrostatic effects plays prominent role in determining electrowetting property. The industrial application of electrowetting is not limited to optics, lenses, display technology, etc.

1.2   Microfluidics

Microfluidics refers to a microscale technology that control and manipulate fluids that are geometrically constrained to a small, sub-millimeter scale [15] and deliver greater efficiency in existing processes such as smaller sample and solvent volumes, higher throughput, faster sequences, and lower costs. It involve study how behavior of fluids at the microscale changes, and how they can be exploited for new uses by integrating various microfluidic factors such as surface tension, energy dissipation, and fluidic interaction. Figure 1.4 shows the various microfluidic platform.

Microfluidic platform

| Capillary driven | ——— | Pressure driven | ——— | Centrifugal driven |

| Electrokinetic driven | ——— | Acoustic driven | ——— | Droplet driven |
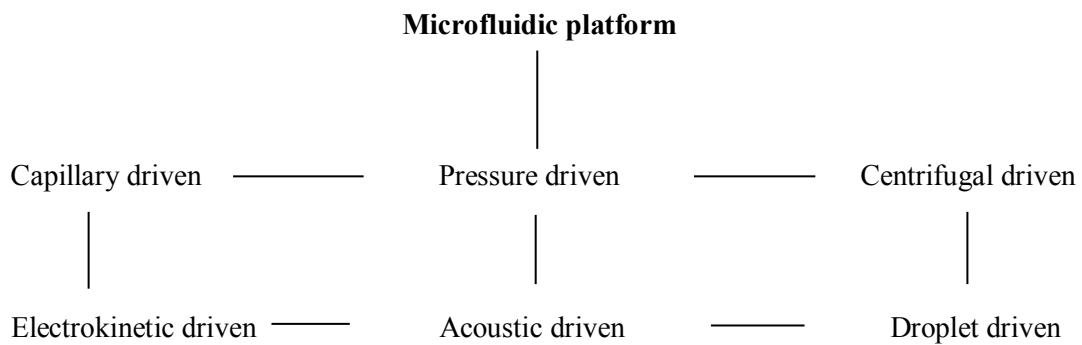
Figure 1.2 Representation of the various microfluidic platform.
Picture produced based on reference [16].

1.2.1   Micro-total-analysis-system (µTAS)

Micro-total-analysis-system [17] represent an automated and integrated analysis of the target analyte in a sample matrix with the method of design, manufacturing and formulating devices [17, 18] that deal with volumes of fluid on the order of nanolitres or picolitres and dimension range from millimeters to micrometers. Figure 1.5 represent the classification scheme for microfluidic mixing based on electrokinetics. It provide a range of advantages such as reduction in consumption of various reagents and chemical waste, a more rapid analysis, a significant improvement in performance, low production cost, portable and disposable after diagnostic use.

4

Electrokinetic mixing

Passive mixing

Active mixing

DC Electroosmosis (EO)

Laminar mixing

Chaotic mixing

Chaotic mixing

Periodically-switching
DC Electroosmosis

Multiple Parallel Stream

Split and recombination

Dielectrophoresis

Electrowetting

AC EK Instability

Surface charge patterning

DC Electrokinetic Instability

Field Induced EO
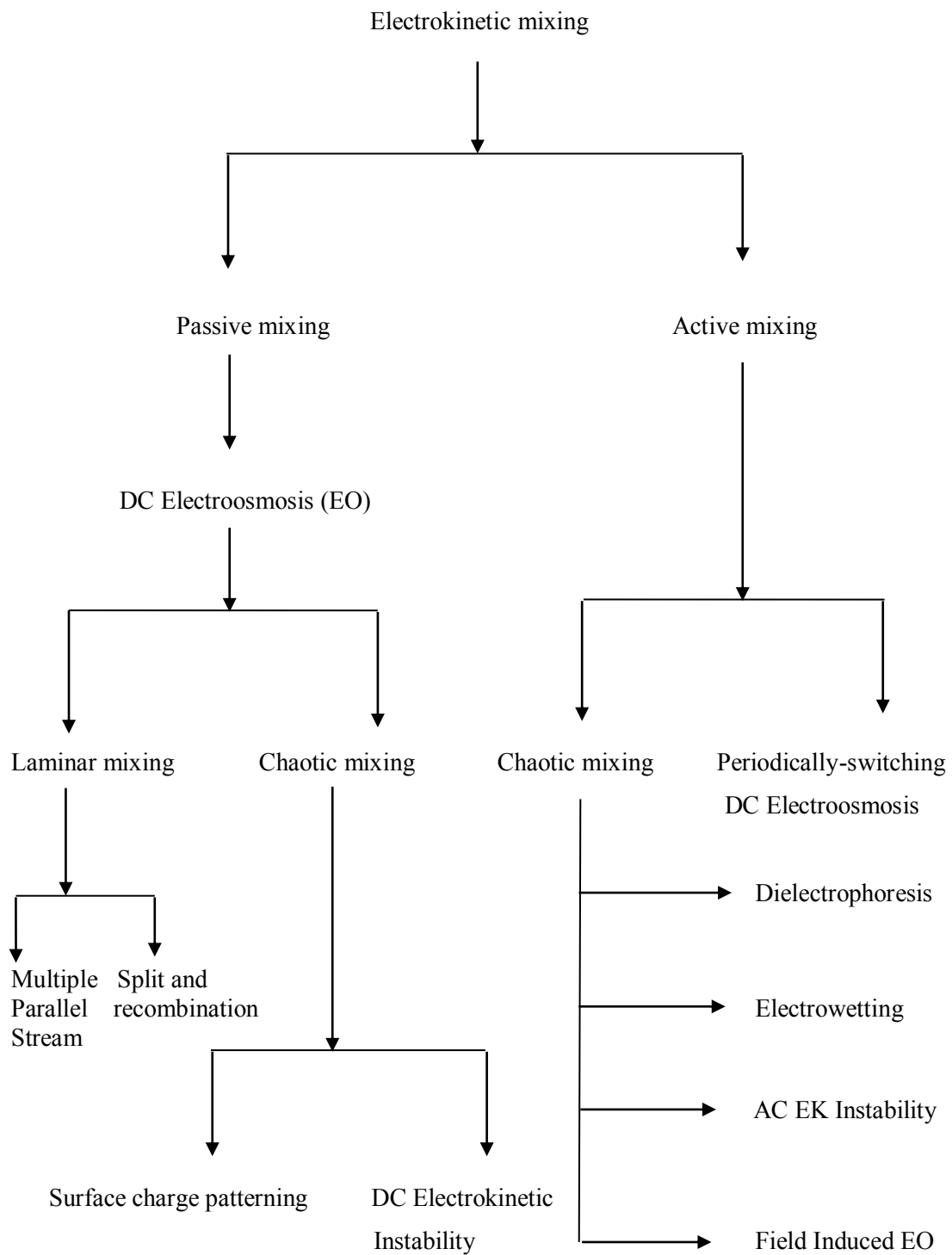
Figure 1.3 Flow chart on classification scheme for microfluidic mixing based on electrokinetics. Diagram produced based on reference [1].

1.2.2 Principle of mixing

Repeated stretching, curve and twisted channels [19], heterogeneous and homogeneous combination surface patch [20] and fluid elements folding within microfluidic mixing arms results an efficient mixing of different concentration solution within micrimixer. An effective microfluidic system must deliver greater contact efficiency, lesser process time, rapid mixing, no unwanted reaction and inconsistenies, etc. Electrokinetic mixing is categorized based on its methodology as active or passive mixing.

1.2.2.1 Passive mixing

Passive mixing refers to the mixing enhancement in pressure-driven micro systems [1, 21] by virtue of their particular geometry dimension, surface and/or instability phenomenon which occurs naturally under a DC electric field.

1.2.2.2 Active mixing

Active or chaotic mixing refers to the mixing enhancement in electrokinetically-driven micro systems using a stationary or time-dependent electric field by means of an externally time-dependent or independent electrical force [22, 23]. Normally, chaotic mixing is achieved by applying following transport technique such as dielectrophoretic (DEP) force perturbation, electrowetting-based droplet, DC/AC electrokinetic instability, field-induced electroosmosis, and surface charges patterning.

1.3 Zeta potential

Zeta potential represent physical property which is exhibited by any charge particle in suspension. It is the electric potential at the interfacial double layer at the location of the slipping plane relative to the point in the bulk fluid away from the interface [24]. Figure 1.6 depicts the zeta potential. In other words, it denotes the stationary layer of fluid attached to the disperse particles and the dispersion medium's potential difference. It is widely used for the quantification of the charge since the net electrical charge is contained within a region bounded by the slipping plane and location of that plane. Stern potential or electric surface potential and zeta potential in a double layer are defined in different locations, they exhibit different (not equal) quantity.
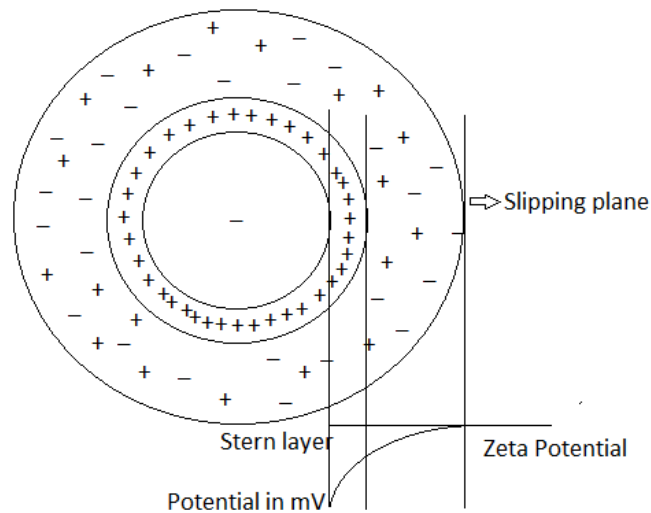
Figure 1.4 Illustration of the zeta potential.
Diagram produced based on reference [24].

Zeta potential is only available path for characterization of double layer property and a key indicator for stability in colloidal dispersion. Magnitude of zeta potential indicates the degree of the electrostatic repulsion or attraction in the dispersion among neighboring equal charged particles. A high zeta potential will confer stability i.e. the solution or dispersion will resist aggregation within molecules and particles that are small enough. When the potential is small, the attractive forces may exceed this repulsion and the dispersion may break and flocculate. Hence particles with high zeta potentials are electrically stabilized whereas with low zeta potentials tend to coagulate or flocculate as shown in the table. Zeta potential is not measurable directly and can be calculated using theoretical and experimentally models.

R. J. Hunter [24] describes the range and characteristic stability property of zeta potential in table 1.1. Here, the author describes that at lower zeta potential range i.e. $\pm$ 0 to $\pm$ 10 mV the colloidal solution shows high instability whereas with increasing zeta potential, the stability of the colloidal solution increase, high stability among $\pm$ 60 to $\pm$ 100 mV.

Table 1.1 Data on zeta potential range and its characteristic property.
Data based on the work of R. J. Hunter [24].

Zeta Potential Range	Characteristics
± 60 to ± 100 mV	High Stability
± 30 to ± 60 mV	Stable
± 10 to ± 30 mV	Unstable
± 0 to ± 10 mV	High Instability

Chapter 2

Literature review

Miniaturization shows an industrial drift from past several years with an automated and integrated microfluidic systems. The microfluidic device engrosses high output with accuracy, precision, and operationality for many processes employing reduce size, shape and quick samples analysis. Lab-on-a-chip devices possess varied characteristic property ranging from silicon/glass closed channels, PDMS/PMMA polymeric matrix, with volumes capacities within the range of micro and nanolitres. This miniaturization of lab-on-a-chip devices plays a fundamental role in the physical and physicochemical property such as surface-to-volume ratio, homogeneous and heterogeneous surfaces, and surface energies within microstructure. The application of microfluidic systems can cover a vast research field such as immunology, macromolecules analysis, biomedical diagnostics, etc.

The first report on electrokinetic application in lab on chip microfluidic devices can be traced back to Chang et al. [1] work in 2007 in which the recent advancements in the micro-mixing based on electrokinetics, including dielectrophoresis, and electroosmosis were reported. Electrokinetic based microfluidic systems serve as an important means for chemical and biological assays since it is portable with low voltage and no external mechanical device usage. Researchers has demonstrated that micromixers must function under low Reynolds numbers and high Péclet numbers conditions. Due to the low Reynolds numbers flows within micromixers, mixing is mostly aided by diffusion, unless otherwise augmented by additional methods. Passive mixers accomplish mixing in DC fields in presence of varied geometric dimension, diverse surface and electrokinetic instability whereas active mixers employs time dependent or independent external electric fields. To achieve high mixing efficiency, microstructure must consist of different mixing techniques

in order to achieve device merits, mainly, microfabrication process, cost effective and high throughput.

Fu et al. [25] has reported a novel microfluidic mixer utilizing electrokinetic driving force under low switching frequency to mix electrolytic fluid samples rapidly and efficiently in a double-T-form microfluidic mixer in 2005. For the mixing purpose, a single high-voltage power source is applied in order to increase the contact area and samples time and perturbations of the fluid field. The intensity distribution downstream from the mixer, is calculated, and the effectiveness of the mixer which is the function of 2 Hz periodic switching frequency and 100 V/cm electric field strength were determined. Various numerical results ascertain the efficiency of double-T-form micromixer high mixing efficiency up to 95% within a mixing length of 1000 mm downstream from the secondary T-junction. In a 150 V/cm driving electric field, the mixing performance were achieved if a longer channel length and a higher switching frequency are applied.

In 2002, Erickson et al. [20] demonstrated an influence of surface heterogeneity on microfluidic mixing employing electroosmotic flow. Researchers have incorporated oppositely charged surface heterogeneities to microchannel walls within the micromixer verified using 3D model and experimental T-shaped mixer. The authors reported that mixing efficiency were greatly improved in presence of surface heterogeneity, highest amongst increased quantity of the surface walls, its size and the degree of heterogeneity respectively, with decrease in the mixing channel length by 70%.

Wang et al. [26] in 2007 reported asymmetric flow geometries and relay switching for microfluidic mixer employing electrokinetics. Mixing is enhanced by employing asymmetric flow geometries and electrokinetic relay actuation within hybrid mixer. Modeling results indicated that electrokinetic relay at an appropriate frequency, asymmetric flow geometries and narrow channel can improve mixing efficiency of a hybrid mixer. A high mixing efficiency up to 95.6% was reached within one sec at 500 μm for a 50 μm wide channel causing rapid mixing of liquids with reduce analysis time and high throughput permit.

Kim et al. [27] have reported a protein concentration device using a reversibly bonded glass/polydimethylsiloxane chevron shaped microfluidic chip with 20 μm distance between the microchannels in 2006. Negatively charged proteins were concentrated under the

influence of an electric field across thin walled microchannel. Different concentrated proteins were separated, due to PDMS dielectric breakdown triggering a nanoscale channel route between the PDMS and the glass, by switching the direction of the electric field parallel to the thin walled section. The reported microfluidic system can be employed as an efficient protein assay. On similar principle as reported by Kim et al. [27], an integrated micro-nanofluidic system for protein analysis, preconcentration and preparation of sample were reported by Anwar et al. [28] in 2011. Here, proteins were trapped electrokinetically near the junction, making the chip an efficient protein preconcentrator. Also, no nano-lithography fabrication methods were used in protein preconcentration signifying great advantage of this integrated micro-nanofluidic system.

Coleman et al. [29] in 2006 has reported symmetric sequential injection and expansion for high efficiency electrokinetic micromixing. This chips were designed with input from a numerical study, microfabrication in polydimethylsiloxane using soft-lithography, and fluorescence microscopy testing. Rapid switching of the electric field greatly improve initial mixing over static-field mixing suggesting efficient mixing strategy for electrokinetic flows. Here, researchers have demonstrated a field switching microfluidic mixing strategy utilizing a symmetric sequential injection geometry with an expansion chamber to achieve high efficiency. Decrease in Péclet number and rapid axial diffusive mixing were enhanced by three-inlet injector connected with two dissimilar incoming solutions whereas downstream injector, the sequence enters an expansion chamber. This sequential injection and expansion with micromixing imparts compact axial length, high mixing efficiency, steady outflow velocity and concentration.

Zhang et al. [30] reported Silicon On Insulator (SOI) processing of a ring electroosmotic micromixer, employing electrodes arrangement and flow obstacles to induce chaotic mixing within a micromixer in 2004. The fabrication process involve heavily doped silicon, and SOI wafer for electrical isolation from the substrate by thermally growing SiO_2 between the two areas to bridge the empty space. Integrated electrodes were fabricated by SOI and the Focused Ion Beam (FIB) processing within full depth microfluidic system. 2D and 3D simulation results represent chaotic mixing application.

A very recent approach for design and simulation of drug mixing and droplets generation employing cell-based digital microfluidic chip were reported by Dong et al. [31] in 2012. Here, researchers has demonstrated that mixing efficiency can be increased by employing

the non-clogging counter-flow microconcentrator. In addition to mixing efficiency, researchers also proposes pressure variation in water and air inlet analysis during a period of droplet generation. To optimizing the microfluidic chip design, simulation work were performed. The microfluidic chip enable cells mixing with drugs within counter flow unit and T-junction, resulting liquid droplets in the moving air flow. Within the frequency range of 25-100Hz, the relation between droplet length and flow rate ratio were found. At droplet length of 160μm, the droplet formation stability is reached at Qd/Qc=1. Glucose solutions of 0.3mol/dm3 and 0.15mol/dm3 concentration were mixed with pressure over 25% or 80% respectively of the max pressure reached. The outlet with a concentration of 0.228mol/dm3 signifies a steady state condition for equal flow-rates within microfluidic chip.

Chapter 3

Simulation

3.1   COMSOL Multiphysics

COMSOL Multiphysics represent fully integrated software suite employing finite element based engineering tool that allowed entering coupled systems of partial differential equations in order to simulate and analyze the multiphysics phenomenon. FEMLAB is a collaborative software involving Finite Element Method (FEM) in adaptive form with automatic error control for the simulation of ordinary and partial differential equations. This software possess a wide range of applicability such as heat transfer, mass-energy transfer, fluid dynamics, general physics, etc.

Finite element method or finite element analysis (FEA) segments a large numerical problem into smaller, simpler parts (finite elements) for finding approximate solutions to boundary value problems for partial differential equations. Simulation workflow involve modeling steps from one and the same environment, mainly,

- Set up model environment
- Create geometric objects
- Specify material properties
- Define physics boundary conditions
- Create the mesh
- Run simulation
- Postprocess the results

Simulation has been performed in COMSOL Multiphysics 5.0 for modeling of electrokinetic mixing using electro-osmotic stationary and time-dependent micropumps via alternate zeta potential patches on the lower surface of the mixing chamber in lab on chip microfluidic device.

3.2 Method and Model
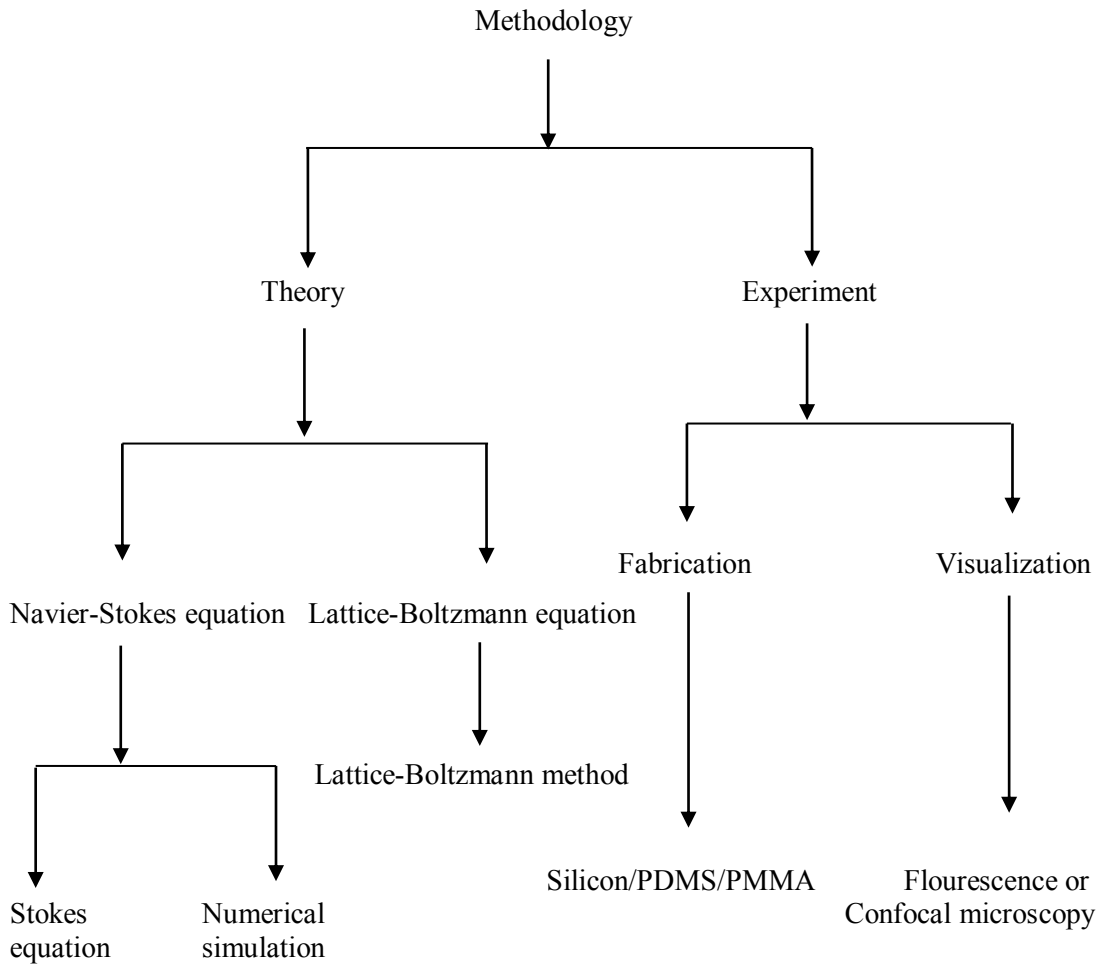
Figure 3.1 Flow chart on methodology classifications for the study of micro-mixing.
Flow chart produced based on reference [1].

3.2.1 Model parameter

Table 3.1 Data on model parameter.

Name	Expression	Value	Description
U0	0.1[mm/s]	1.0000E-4 m/s	Mean inflow velocity
sigma_w	2.0[S/m]	2.0000 S/m	Conductivity of the ionic solution
eps_r	45	45.000	Relative permittivity of the fluid
zeta	25mV / 50mV / 100mV	25mV / 50mV / 100mV	Zeta potential
V0	25mV / 50mV / 100mV	25mV / 50mV / 100mV	Maximum value of the AC potential
omega	2*pi[rad]*8[Hz]	50.265 Hz	Angular frequency of the AC potential
D	1e-11[m^2/s]	1.0000E-11 m²/s	Diffusion coefficient of the ionic solution
c0	1[mol/m^3]	1.0000 mol/m³	Initial concentration
t	0[s]	0.0000 s	Start time

3.2.2 Model physics

Table 3.2 Data on model physics.

Physics interface
Laminar Flow (spf)
Electric Currents (ec)
Transport of Diluted Species (tds)

3.2.3 Model mesh

Various mesh element types for electroosmotic simulation:

2D models - Triangular and Quadrilateral.

3D models - Tetrahedral, pyramids, bricks, and prisms.

Tetrahedral elements (simplex) represent the 3D default element type within COMSOL Multiphysics with adaptive mesh refinement. The other three element types i.e. pyramids,

bricks, and prisms involve high meshing algorithm and user input, and unable to mesh a particular geometry.

2D models environment consist of 22 vertex elements, 22 boundary elements, 20 element number, 0.2 maximum element size, 1.1 maximum element growth size and 0.005468 minimum element quality with triangular mesh whereas 3D models environment consist of around 300000 elements, around 1100000 degrees of freedom, 64 vertex elements, around 2500 edge elements with tetrahedral mesh.

Table 3.3 Data on 3D mesh size.

Name	Value
Maximum element size	130
Minimum element size	2
Curvature factor	0.6
Resolution of narrow regions	0.5
Maximum element growth rate	1.5
Custom element size	Custom

Mesh density is higher near the zeta potential patch both in 2D and 3D model which increase the high surface area, contact and mixing efficiency between two solutions.

3.2.4   Electroosmotic simulation

Mechanism:

Electroosmotic flow induce circulating motion by the application of an alternate AC zeta potential field across a micromixer. The applied electric field exert a force on free ions in the charged Debye layer, and induces a flow velocity which is proportional to this electric field. It gives rise to hydrodynamic uncertainties via circulating flows resulting increase contact efficiency of the reagent and analyte and hence enhancing the mixing efficiency by an order of magnitude or more over pure diffusion.

Equations:

The Navier-Stokes equation for incompressible flow describe the flow in the channels. This equation can be expressed based on references [32, 33].

$$\rho(\ \partial v/\partial t + (v.\nabla)v\ ) = -\nabla p + \mu\nabla 2\ v + f \qquad [1]$$

Where

$\partial v/\partial t$	=	Unsteady acceleration
$(v.\nabla)v$	=	Convective acceleration
$\rho(\partial v/\partial t + (v.\nabla)v)$	=	Inertial term
$-\nabla p$	=	Pressure gradient
$\mu \nabla^2 v$	=	Viscosity
f	=	External forces
ρ	=	Fluid density

The convection-diffusion equation describes the concentration of the dissolved substances in the fluid inside the rectangular micromixer. This convection-diffusion equation form can be expressed based on reference [33].

$$\partial c/\partial t + \nabla.(-D \nabla_C) = R - u \nabla_C \qquad [2]$$

Where

$\partial c/\partial t$	=	Concentration gradient
c	=	Concentration [mol/m^3]
D	=	Diffusion coefficient of the solution
R	=	Reaction rate (R = 0 since concentration is not affected by any reactions)
u	=	Flow velocity [mm/s]

The simulation model replaces the thin electric double layer with the Helmholtz-Smoluchowski relation between the electro-osmotic velocity and the tangential component of the applied electric field. Helmholtz-Smoluchowski equation can be expressed based on reference [33].

$$u = {}^{\varepsilon}{}_w \zeta \nabla_T V / \eta \qquad [3]$$

Where

u	=	Velocity [mm/s]
ε_w	=	Fluid's electric permittivity [F/m]
ζ	=	Zeta potential at the channel wall [mV]
V	=	Electric potential [mV]
η	=	Dynamic viscosity [kg/ms]

Chapter 4

Experimental results

4.1   2D Simulations Results

4.1.1   2D Model A

With adjacent two opposite electric potential of 25mV, 50mV and 100mV respectively.
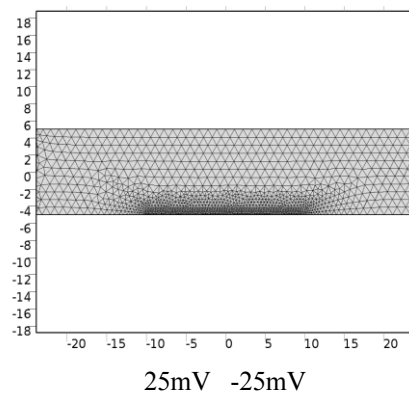

25mV   -25mV

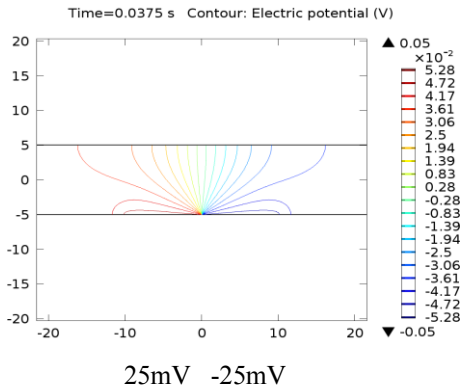**Figure 4.1 Representation of the microchannel meshing.**

Time=0.0375 s   Contour: Electric potential (V)

25mV   -25mV

Figure 4.2 Representation of the two electric potential contour.
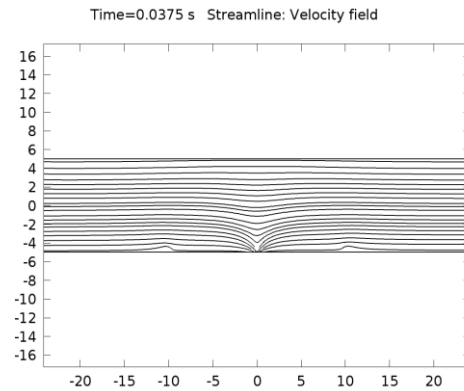

Time=0.0375 s   Streamline: Velocity field

Figure 4.3 Representation of the velocity field streamline in adjacent two opposite electric potential of 25mV and -25mV.

Time=0.0375 s   Streamline: Velocity field

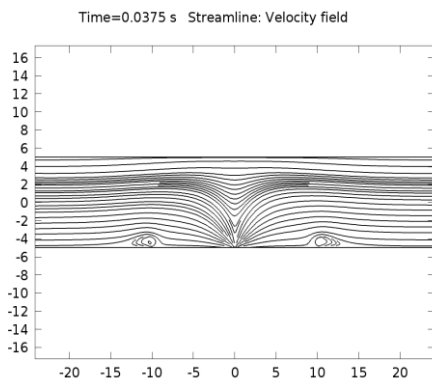**Figure 4.4 Representation of the velocity field streamline in adjacent two opposite electric potential of 50mV and -50mV.**
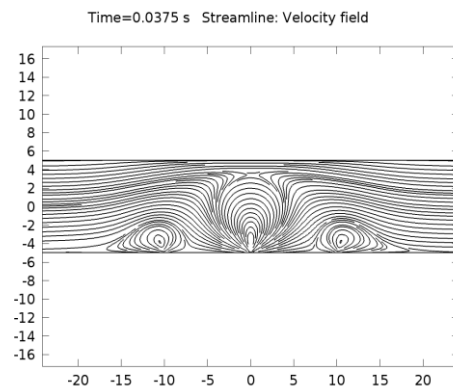

Time=0.0375 s   Streamline: Velocity field

Figure 4.5 Representation of the velocity field streamline in adjacent two opposite electric potential of 100mV and -100mV.

2D Model A Inference:

25mV zeta potential solution shows low streamline velocity field, 50mV zeta potential solution shows slight increase whereas 100mV zeta potential exhibit highest streamline velocity field with 10 μm height micromixer for two adjacent opposite electric potential. Hence, model A shows a cumulative increase in velocity field streamline within micromixer from 25mV up to 100mV zeta potential solution.

4.1.2   2D Model B

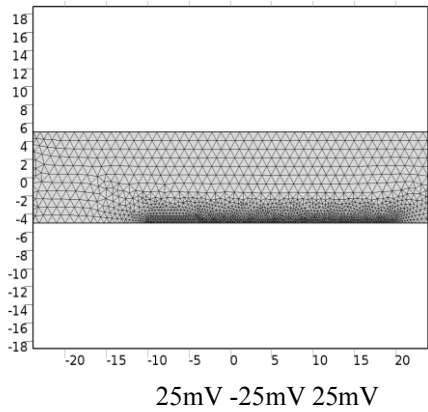With alternate three opposite electric potential of 25mV, 50mV and 100mV respectively.

25mV -25mV 25mV

Figure 4.6 Representation of the microchannel meshing.

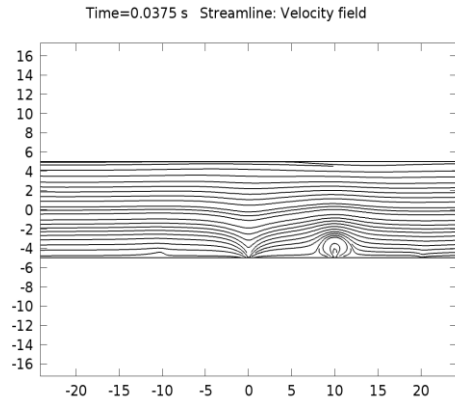**Figure 4.8 Representation of the velocity field streamline with three alternate opposite electric potential of 25mV, -25mV and 25mV.**
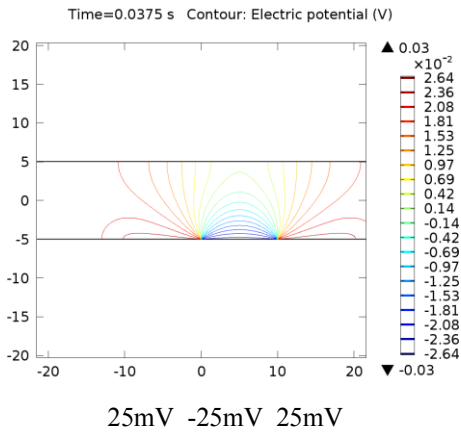

25mV -25mV 25mV
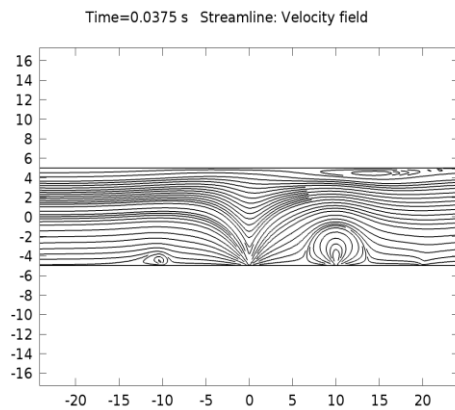
Figure 4.7 Representation of the three electric potential contour.

Figure 4.9 Representation of the velocity field streamline with three alternate opposite electric potential of 50mV, -50mV and 50mV.
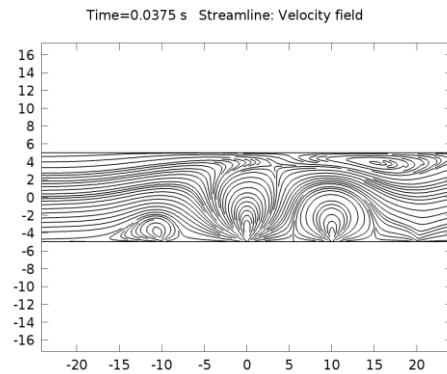
Time=0.0375 s   Streamline: Velocity field

Figure 4.10 Representation of the velocity field streamline with three alternate opposite electric potential of 100mV, -100mV and 100mV.

2D Model B Inference:

25mV zeta potential solution shows low streamline velocity field, 50mV zeta potential solution shows slight increase whereas 100mV zeta potential exhibit highest streamline velocity field with 10 μm height micromixer for alternate three opposite electric potential. Hence, model B shows a cumulative increase in velocity field streamline within micromixer from 25mV up to 100mV zeta potential solution.

4.1.3   2D Model C

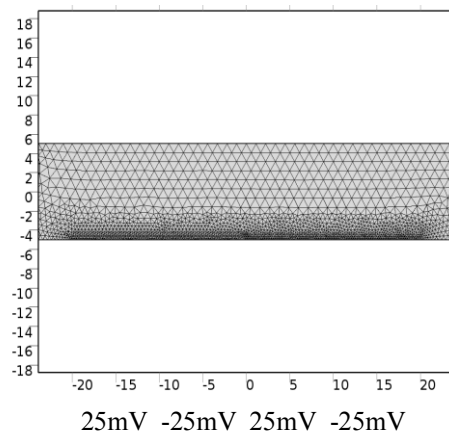With four alternate opposite electric potential of 25mV, 50mV and 100mV respectively.

.

25mV -25mV 25mV -25mV

Figure 4.11 Representation of the microchannel meshing.
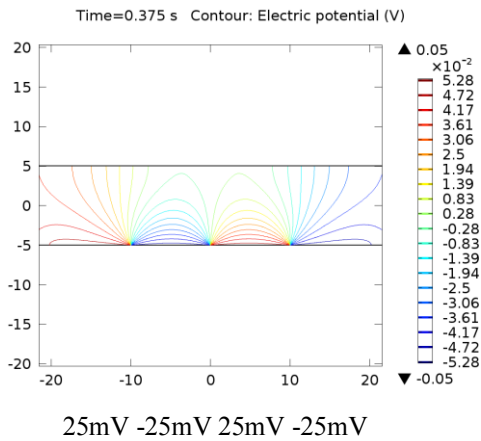
25mV -25mV 25mV -25mV

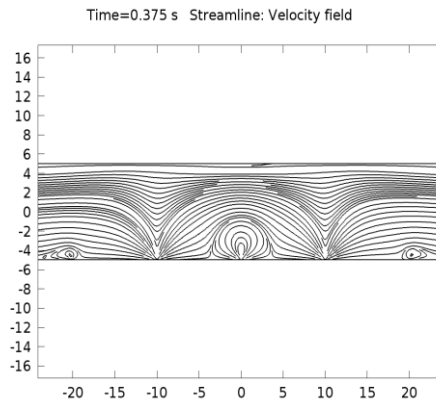**Figure 4.12 Representation of the four electric potential contour.**

Figure 4.14 Representation of the velocity field streamline with four alternate opposite electric potential of 50mV, -50mV, 50mV and -50mV.
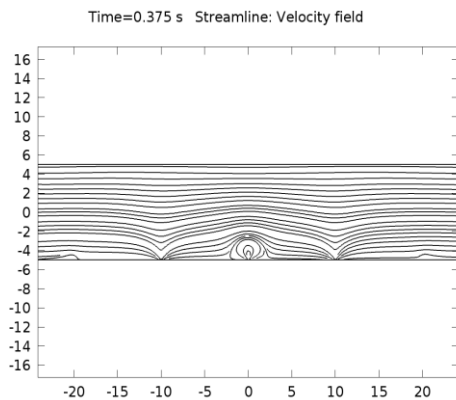

Figure 4.13 Representation of the velocity field streamline with four alternate opposite electric potential of 25mV, -25mV, 25mV and -25mV.
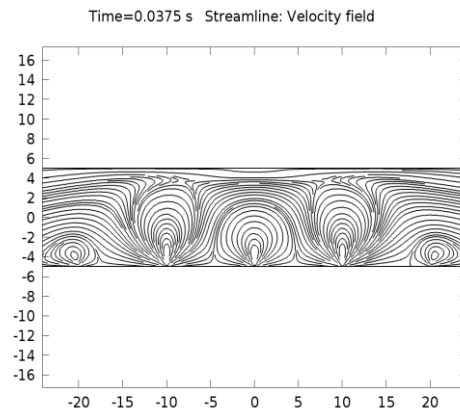

Figure 4.15 Representation of the velocity field streamline with four alternate opposite electric potential of 100mV, -100mV, 100mV and -100mV.

2D Model C Inference:

25mV zeta potential solution shows low streamline velocity field, 50mV zeta potential solution shows slight increase whereas 100mV zeta potential exhibit highest streamline velocity field with 10 μm height micromixer for four alternate opposite electric potential. Hence, model C shows a cumulative increase in velocity field streamline within micromixer from 25mV up to 100mV zeta potential solution.

4.1.4   2D Model D

With alternate four opposite electric potential of 25mV, 50mV and 100mV on lower and upper layers respectively.

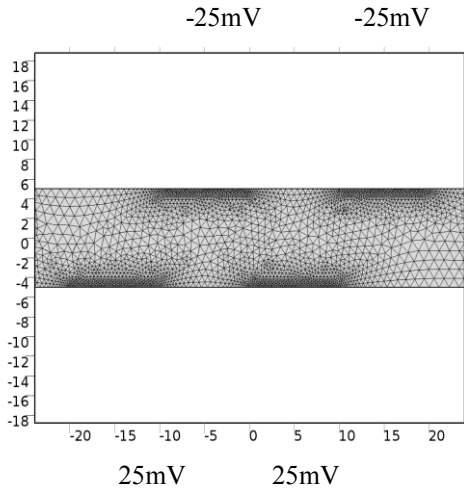-25mV   -25mV

25mV   25mV

Figure 4.16 Representation of the microchannel meshing.

Figure 4.18 Representation of the velocity field streamline with alternate four opposite electric potential on lower and upper layers of 25mV, -25mV, 25mV and -25mV.

-25mV   -25mV

25mV   25mV

Figure 4.17 Representation of the four electric potential contour.
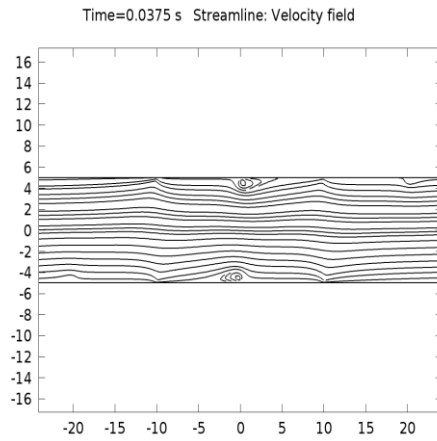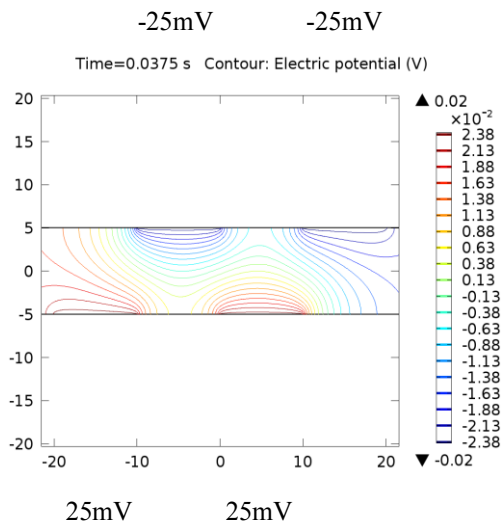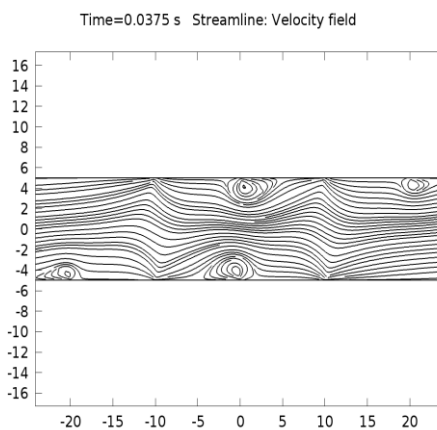

Figure 4.19 Representation of the velocity field streamline with alternate four opposite electric potential on lower and upper layers of 50mV, -50mV, 50mV and -50mV.
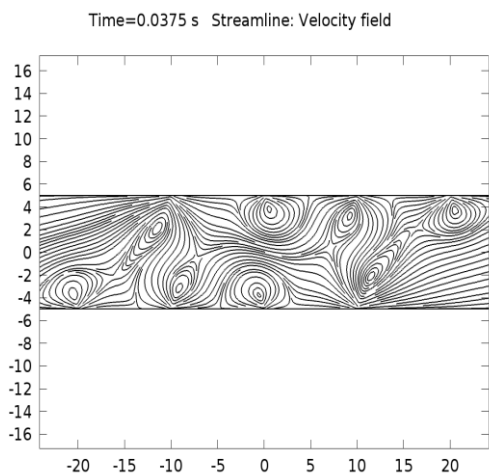
23

Time=0.0375 s Streamline: Velocity field

Figure 4.20 Representation of the velocity field streamline with alternate four opposite electric potential on lower and upper layers of 100mV, -100mV, 100mV and -100mV.

2D Model D Inference:

25mV zeta potential solution shows low streamline velocity field, 50mV zeta potential solution shows slight increase whereas 100mV zeta potential exhibit highest streamline velocity field with 10 µm height micromixer for four alternate opposite electric potential on lower and upper layer. Hence, model D shows a cumulative increase in velocity field streamline within micromixer from 25mV up to 100mV zeta potential solution.

4.1.5   2D Model E

T-shaped micromixer with adjacent opposite electric potential of 25mV, 50mV and 100mV respectively.
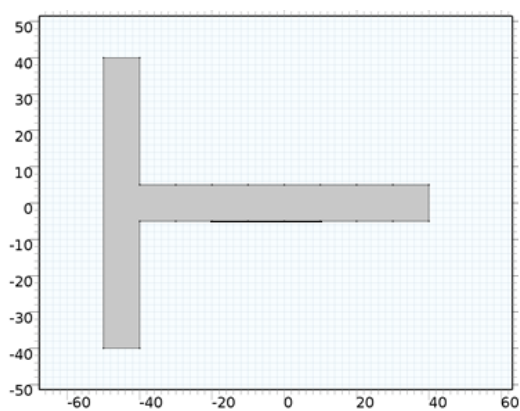
25mV -25mV 25mV

Figure 4.21 Representation of the T-shaped microchannel three electric potential placing.
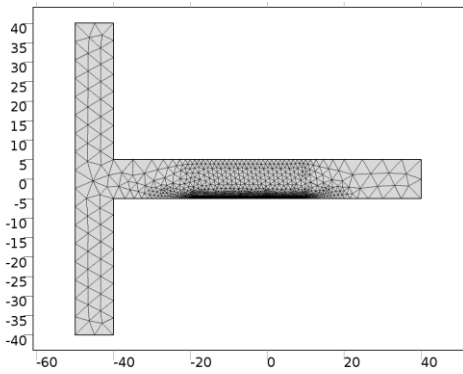
Figure 4.22 Representation of the T-shaped microchannel meshing.

Figure 4.23 Representation of the T-shaped microchannel three electric potential.

Figure 4.24 Representation of the T-shaped microchannel surface concentration with adjacent three opposite electric potential of 25mV, -25mV and 25mV respectively.

Figure 4.25 Representation of the T-shaped microchannel surface concentration and velocity field streamline with adjacent three opposite electric potential of 25mV, -25mV and 25mV respectively.

Figure 4.26 Representation of the T-shaped microchannel surface concentration with adjacent three opposite electric potential of 50mV, -50mV and 50mV respectively.
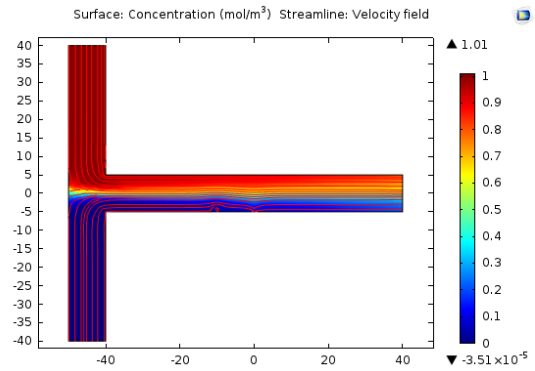
25

Figure 4.27 Representation of the T-shaped microchannel surface concentration and velocity field streamline with adjacent three opposite electric potential of 50mV, -50mV and 50mV respectively.
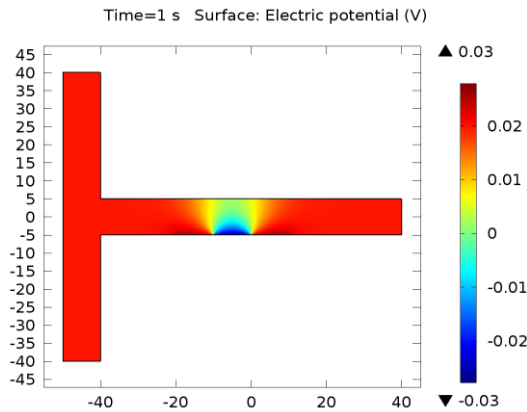
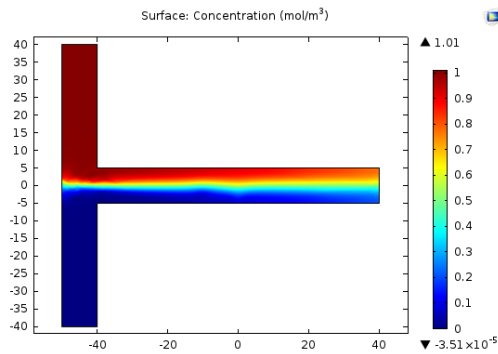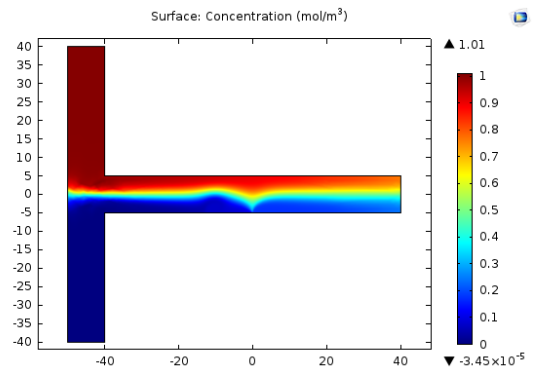**Figure 4.28 Representation of the T-shaped microchannel surface concentration with adjacent three opposite electric potential of 100mV, -100mV and 100mV respectively.**
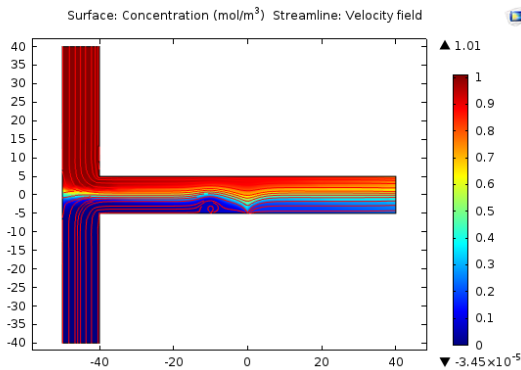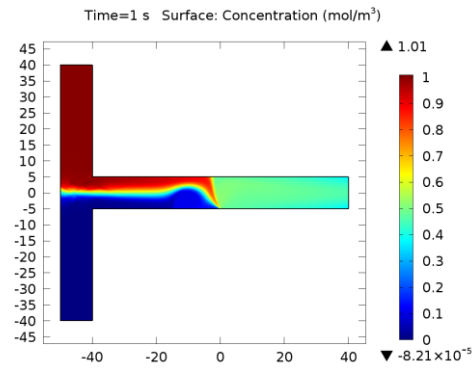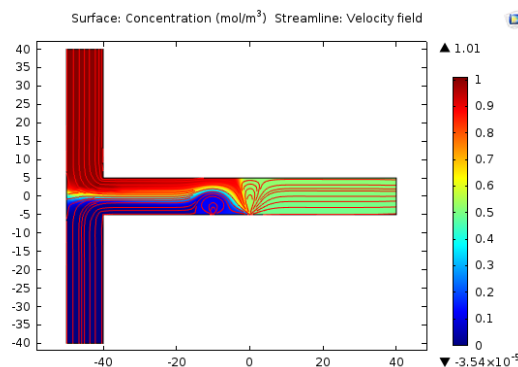

Figure 4.29 Representation of the T-shaped microchannel surface concentration and velocity field streamline with adjacent three opposite electric potential of 100mV, -100mV and 100mV respectively.

2D Model E Inference:

In T-shaped microfluidic micromixer with three alternate opposite electric potential, 25mV zeta potential solution shows low mixing efficiency and streamline velocity field, 50mV zeta potential solution shows slight increase in mixing efficiency whereas 100mV zeta potential exhibit highest and complete mixing (0.5 mol/m^3) and streamline velocity field with 10 µm height micromixer for concentration 1 mol/m^3 and 0 mol/m^3 respectively. Hence, model E shows a cumulative increase in mixing efficiency within micromixer from 25mV up to 100mV zeta potential solution, where 100mV zeta potential exhibit highest concentration mixing of 0.5 mol/m^3.

4.1.6 2D Model F

T-shaped micromixer with four alternate opposite electric potential of 25mV, 50mV and 100mV respectively.
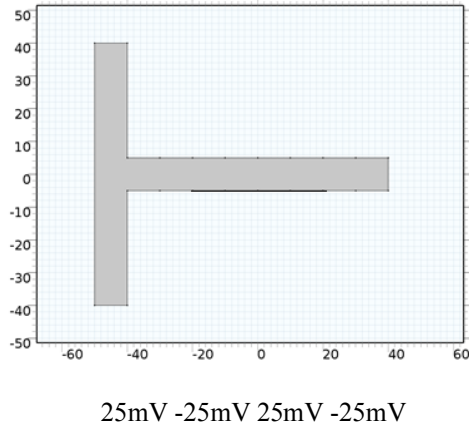

25mV -25mV 25mV -25mV

Figure 4.30 Representation of the T-shaped microchannel four electric potential placing.
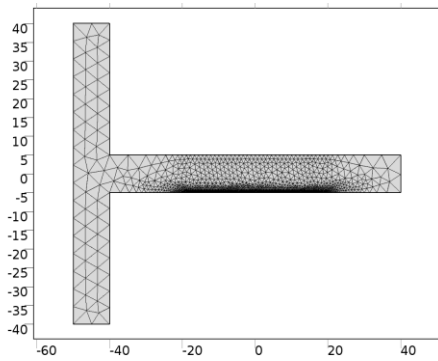
Figure 4.31 Representation of the T-shaped microchannel meshing.
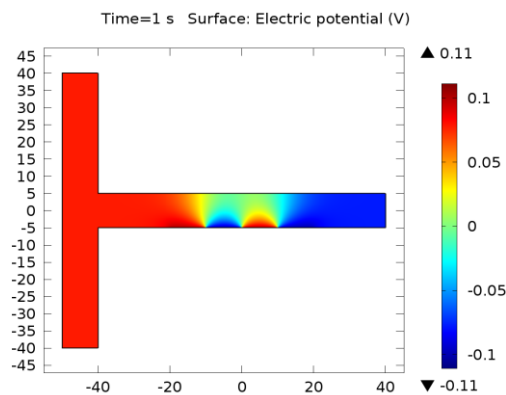
Figure 4.32 Representation of the T-shaped microchannel four electric potential.

Figure 4.33 Representation of the T-shaped microchannel surface concentration with four alternate opposite electric potential of 25mV, -25mV, 25mV and -25mV respectively.

Figure 4.34 Representation of the T-shaped microchannel surface concentration and velocity field streamline with four alternate opposite electric potential of 25mV, -25mV, 25mV and -25mV respectively.

27

Figure 4.35 Representation of the T-shaped microchannel surface concentration with four alternate opposite electric potential of 50mV, -50mV, 50mV and -50mV respectively.

Figure 4.36 Representation of the T-shaped microchannel surface concentration and velocity field streamline with four alternate opposite electric potential of 50mV, -50mV, 50mV and -50mV respectively

Figure 4.37 Representation of the T-shaped microchannel surface concentration with four alternate opposite electric potential of 100mV, -100mV, 100mV and -100mV respectively.

Figure 4.38 Representation of the T-shaped microchannel surface concentration and velocity field streamline with four alternate opposite electric potential of 100mV, -100mV, 100mV and -100mV respectively.

2D Model F Inference:

In T-shaped microfluidic micromixer with four alternate opposite electric potential, 25mV zeta potential solution shows low mixing efficiency and streamline velocity field, 50mV zeta potential solution shows slight increase whereas 100mV zeta potential exhibit highest and complete mixing (0.5 mol/m^3) and streamline velocity field with 10 μm height micromixer for concentration 1 mol/m^3 and 0 mol/m^3 respectively. Hence, model F

28

shows a cumulative increase in mixing efficiency within micromixer from 25mV up to 100mV zeta potential solution, where 100mV zeta potential exhibit highest concentration mixing of 0.5 mol/m^3.

4.1.7   2D Model G

T-shaped micromixer with five alternate opposite electric potential of 25mV, 50mV and 100mV respectively.

25mV-25mV 25mV -25mV 25mV

Figure 4.39 Representation of the T-shaped microchannel five electric potential placing.
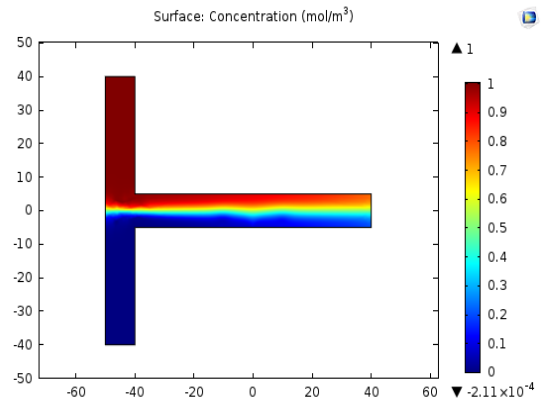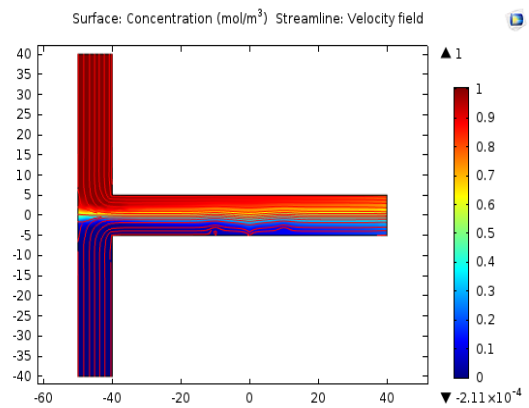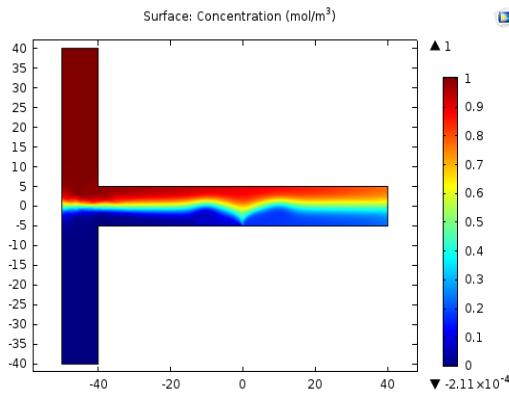

Figure 4.41 Representation of the T-shaped microchannel five electric potential.
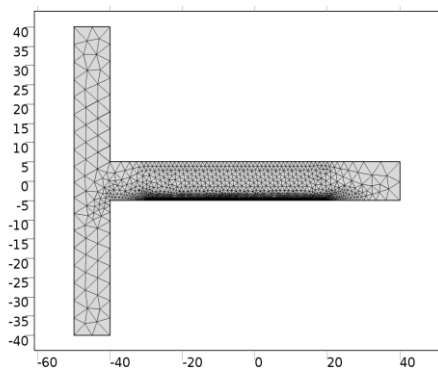
Figure 4.40 Representation of the T-shaped microchannel meshing.

Figure 4.42 Representation of the T-shaped microchannel surface concentration with five alternate opposite electric potential of 25mV, -25mV, 25mV, -25mV and 25mV respectively.
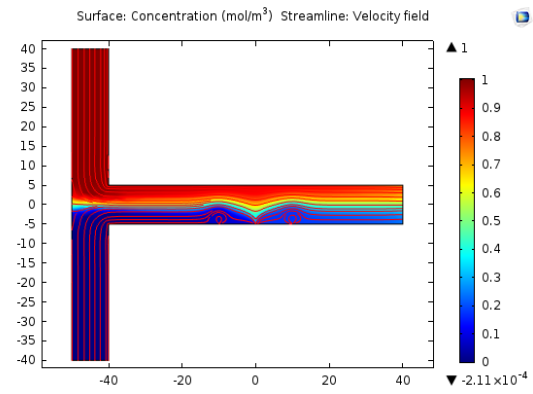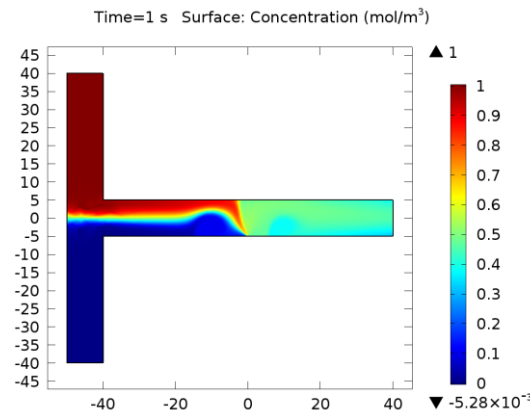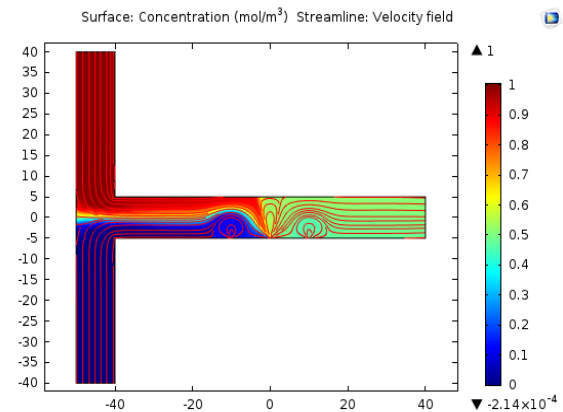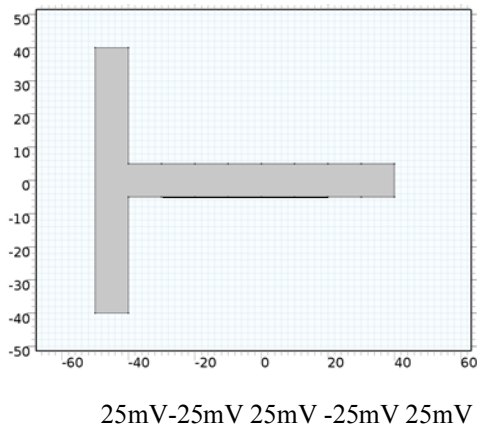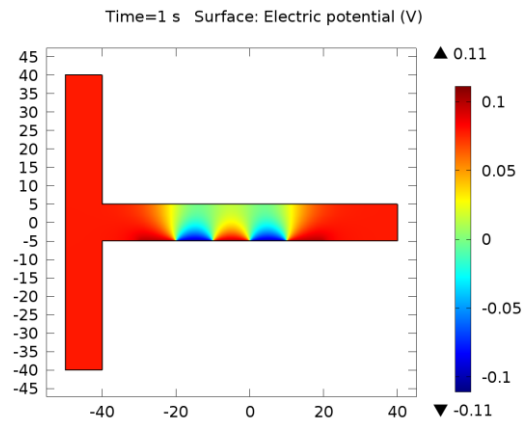
29

Figure 4.43 Representation of the T-shaped microchannel surface concentration and velocity field streamline with five alternate opposite electric potential of 25mV, -25mV, 25mV, -25mV and 25mV respectively.

Figure 4.45 Representation of the T-shaped microchannel surface concentration and velocity field streamline with five adjacent opposite electric potential of 50mV, -50mV, 50mV, -50mV and 50mV respectively.
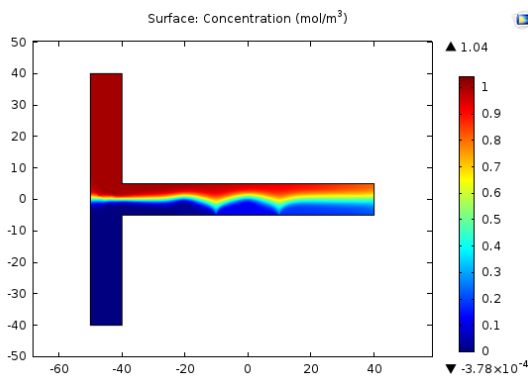
Figure 4.44 Representation of the T-shaped microchannel surface concentration with five alternate opposite electric potential of 50mV, -50mV, 50mV, -50mV and 50mV respectively.
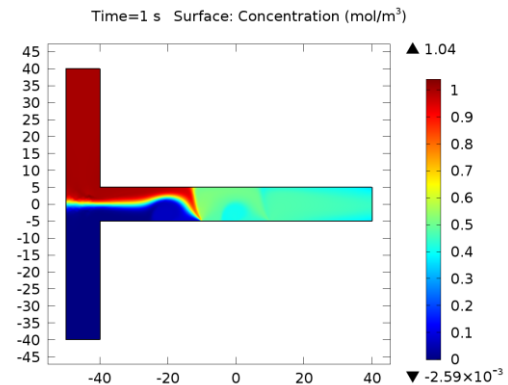
Figure 4.46 Representation of the T-shaped microchannel surface concentration with five alternate opposite electric potential of 100mV, -100mV, 100mV, -100mV and 100mV respectively.
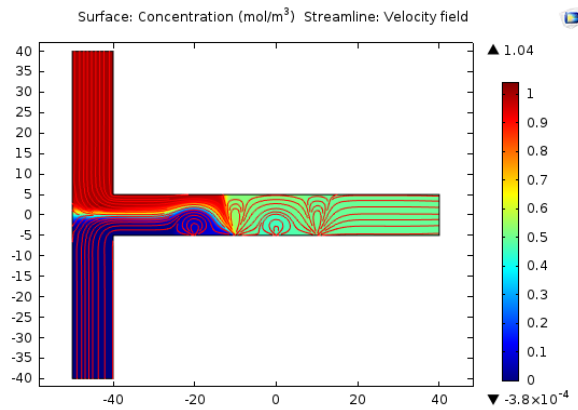
Figure 4.47 Representation of the T-shaped microchannel surface concentration and velocity field streamline with five alternate opposite electric potential of 100mV, -100mV, 100mV, -100mV and 100mV respectively.

2D Model G Inference:

In T-shaped microfluidic micromixer with five alternate opposite electric potential, 25mV zeta potential solution shows low mixing efficiency and streamline velocity field, 50mV zeta potential solution shows slight increase in efficiency whereas 100mV zeta potential exhibit highest and complete mixing (0.5 mol/m^3) and streamline velocity field with 10 μm height micromixer for concentration 1 mol/m^3 and 0 mol/m^3 respectively. Hence, model G shows a cumulative increase in mixing efficiency within micromixer from 25mV up to 100mV zeta potential solution, where 100mV zeta potential exhibit highest concentration mixing of 0.5 mol/m^3.

4.2   3D Simulations Results

4.2.1   3D Model A

T-shaped 3D micromixer with four zeta potential patch of opposite electric potential of 25mV, 50mV and 100mV respectively.

Figure 4.48 Representation of the 3D T-shaped microchannel with four zeta potential patch placing.

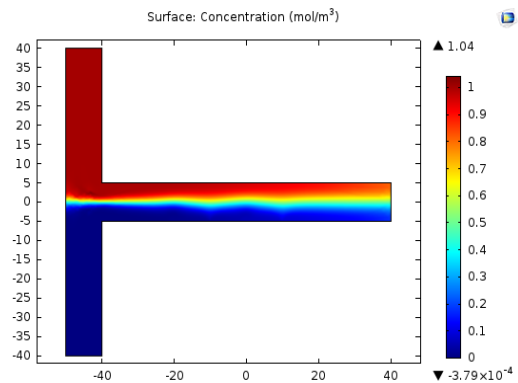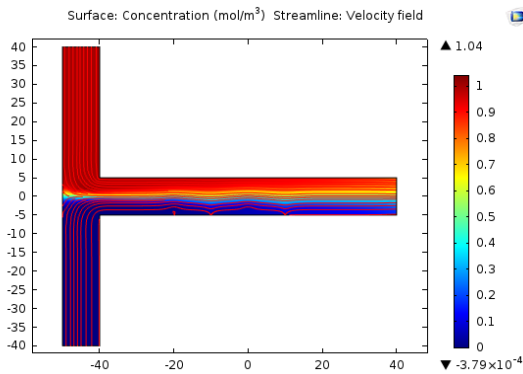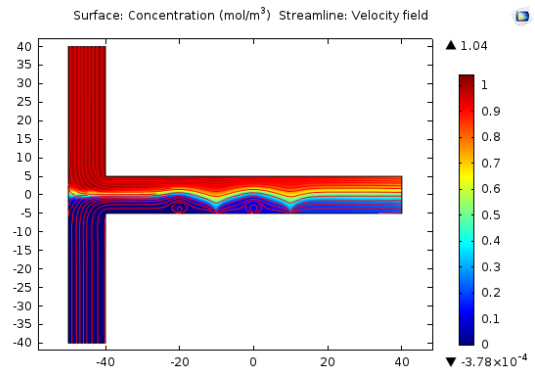**Figure 4.49 Representation of the 3D T-shaped microchannel meshing with four zeta potential patch.**

Figure 4.50 Representation of the 3D T-shaped microchannel with four electric potential.

Figure 4.51 Representation of the 3D T-shaped microchannel surface concentration with four zeta potential patch of electric potential 25mV, -25mV, 25mV and -25mV respectively.

Figure 4.52 Representation of the 3D T-shaped microchannel with isosurface concentration having four zeta potential patch of electric potential 25mV, -25mV, 25mV and -25mV respectively.

Figure 4.54 Representation of the 3D T-shaped microchannel with isosurface concentration having four zeta potential patch of electric potential 50mV, -50mV, 50mV and -50mV respectively.

Figure 4.53 Representation of the 3D T-shaped microchannel surface concentration with four zeta potential patch of electric potential 50mV, -50mV, 50mV and -50mV respectively.

Figure 4.55 Representation of the 3D T-shaped microchannel surface concentration with four zeta potential patch of electric potential 100mV, -100mV, 100mV and -100mV respectively.

Figure 4.56 Representation of the 3D T-shaped microchannel with isosurface concentration having four zeta potential patch of electric potential 100mV, -100mV, 100mV and -100mV respectively.

3D Model A Inference:

In T-shaped 3D microfluidic micromixer with four zeta potential patch of opposite electric potential, 25mV and 50mV zeta potential solutions shows poor mixing efficiency whereas 100mV zeta potential exhibit slight mixing with 30 μm height micromixer for concentration 1 mol/m^3 and 0 mol/m^3 respectively. Hence, model A shows virtually no concentration mixing for 25mV and 50mV zeta potential solution however slight increase in mixing efficiency within micromixer for 100mV zeta potential solution for two different concentration of 1 mol/m^3 and 0 mol/m^3 respectively.

4.2.2 3D Model B

T-shaped 3D micromixer with six zeta potential patch of opposite electric potential of 25mV, 50mV and 100mV respectively.
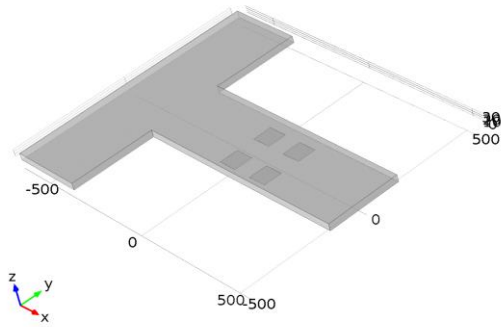

Figure 4.57 Representation of the 3D T-shaped microchannel with six zeta potential patch placing.
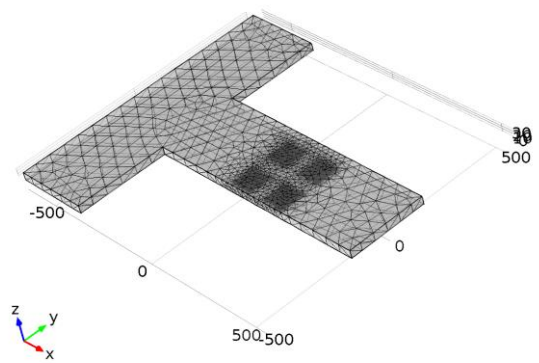
Figure 4.58 Representation of the 3D T-shaped microchannel meshing with six zeta potential patch.
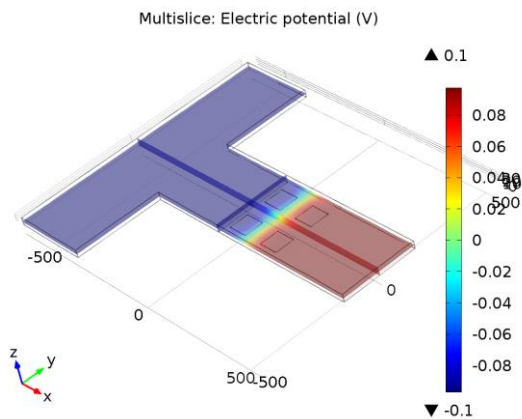

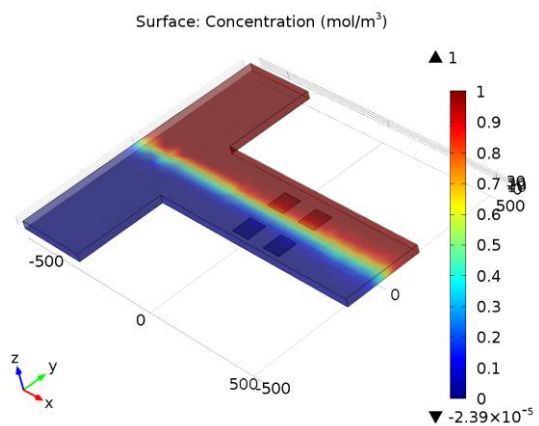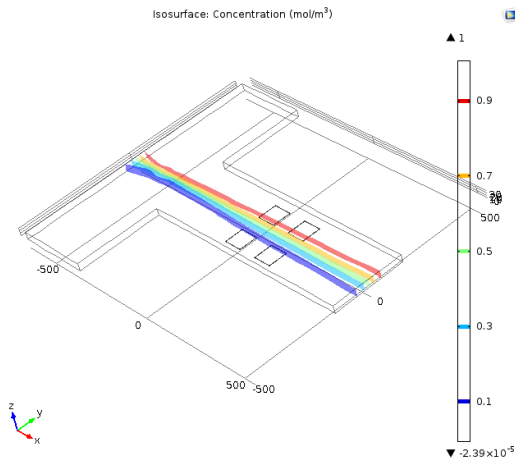**Figure 4.59 Representation of the 3D T-shaped microchannel with six electric potential.**

Figure 4.60 Representation of the 3D T-shaped microchannel surface concentration with six zeta potential patch of electric potential 25mV, -25mV, 25mV, -25mV, 25mV and -25mV respectively.
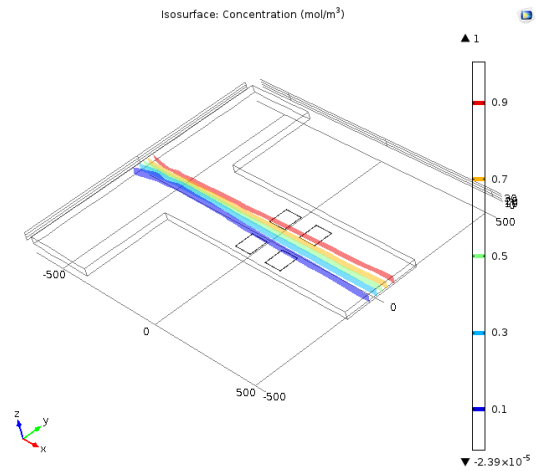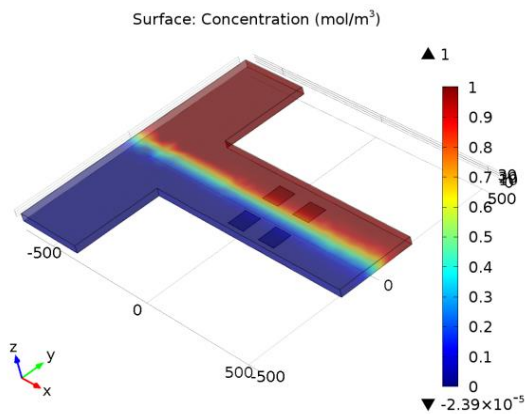

Figure 4.61 Representation of the 3D T-shaped microchannel with isosurface concentration having six zeta potential patch of electric potential 25mV, -25mV, 25mV, -25mV, 25mV and -25mV respectively.
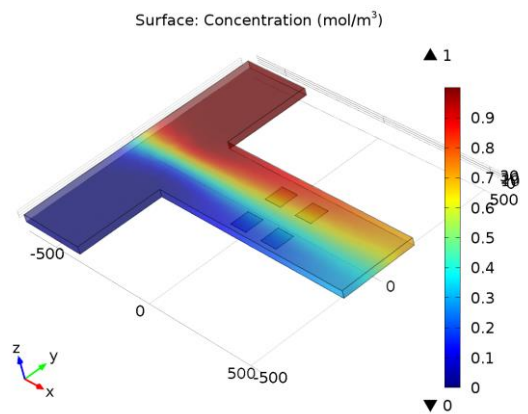

Figure 4.62 Representation of the 3D T-shaped microchannel surface concentration with six zeta potential patch of electric potential 50mV, -50mV, 50mV, -50mV, 50mV and -50mV respectively.
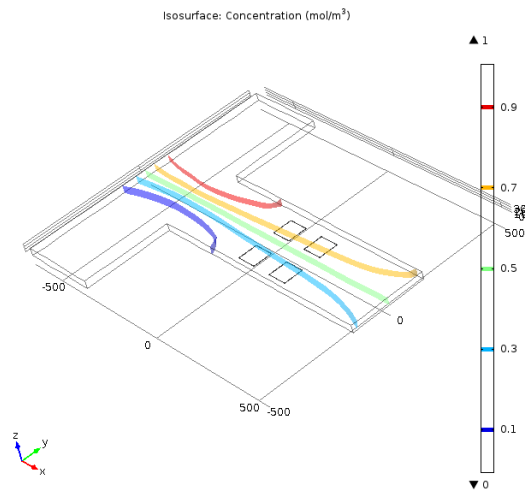
Figure 4.63 Representation of the 3D T-shaped microchannel with isosurface concentration having six zeta potential patch of electric potential 50mV, -50mV, 50mV, -50mV, 50mV and -50mV respectively.

Figure 4.64 Representation of the 3D T-shaped microchannel surface concentration with six zeta potential patch of electric potential 100mV, -100mV, 100mV, -100mV, 100mV and -100mV respectively.

Figure 4.65 Representation of the 3D T-shaped microchannel with isosurface concentration having six zeta potential patch of electric potential 100mV, -100mV, 100mV, -100mV, 100mV and -100mV respectively.

3D Model B Inference:

In T-shaped 3D microfluidic micromixer with six zeta potential patch of opposite electric potential, 25mV and 50mV zeta potential solutions shows poor mixing efficiency whereas 100mV zeta potential exhibit complete mixing with 30 μm height micromixer for concentration 1 mol/m^3 and 0 mol/m^3 respectively. Hence, model B shows virtually no concentration mixing for 25mV and 50mV zeta potential solution however complete mixing

efficiency within micromixer for 100mV zeta potential solution for two different concentration of 1 mol/m^3 and 0 mol/m^3 respectively.

4.2.3   3D Model C

T-shaped 3D micromixer with eight zeta potential patches of opposite electric potential of 25mV, 50mV and 100mV respectively.
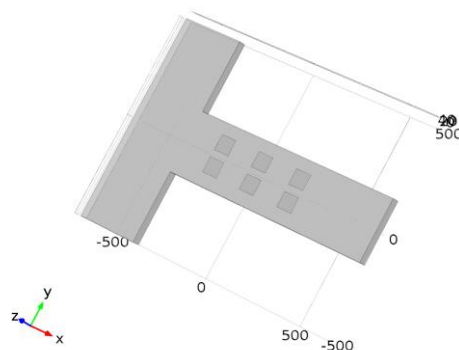

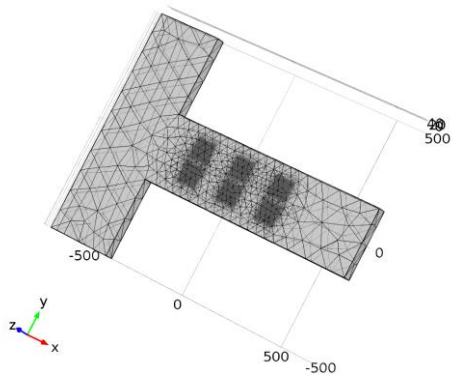**Figure 4.66 Representation of the 3D T-shaped microchannel with eight zeta patch placing.**
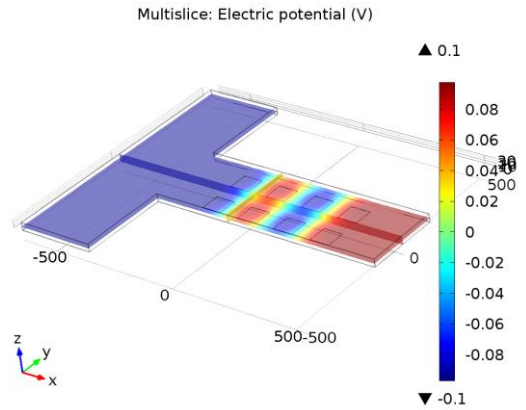
Figure 4.68 Representation of the 3D T-shaped microchannel with eight electric potential.

Figure 4.67 Representation of the 3D T-shaped microchannel meshing with eight zeta potential patch.

Figure 4.69 Representation of the 3D T-shaped microchannel surface concentration with eight zeta potential patch of electric potential 25mV, -25mV, 25mV, -25mV, 25mV, -25mV, 25mV and -25mV respectively.
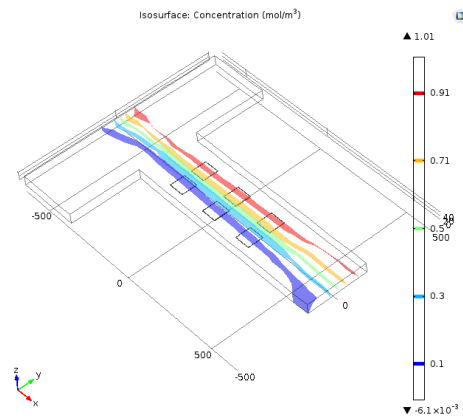
Figure 4.70 Representation of the 3D T-shaped microchannel with isosurface concentration having six zeta potential patch of electric potential 25mV, -25mV, 25mV, -25mV, 25mV, -25mV, 25mV and -25mV respectively.
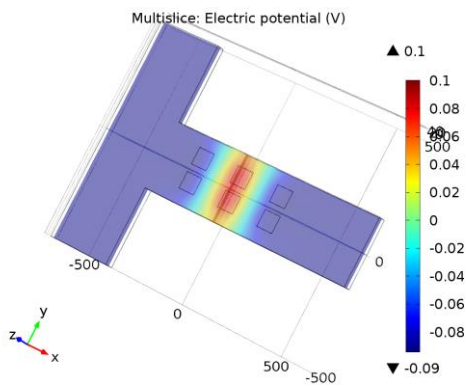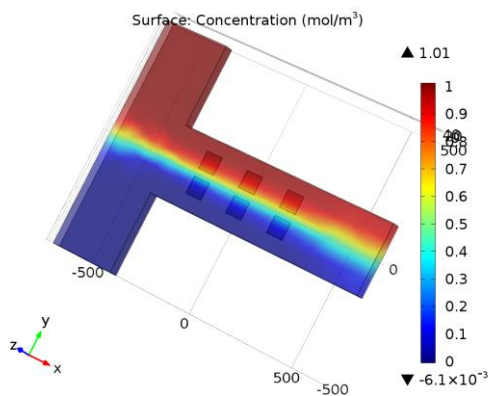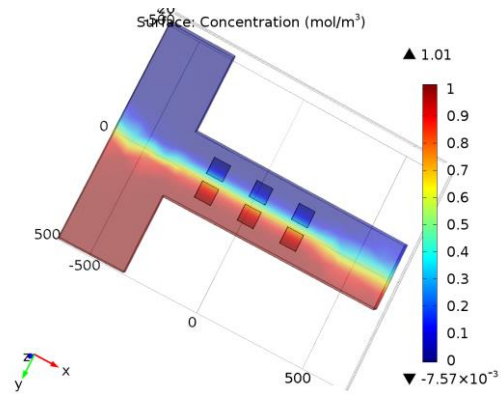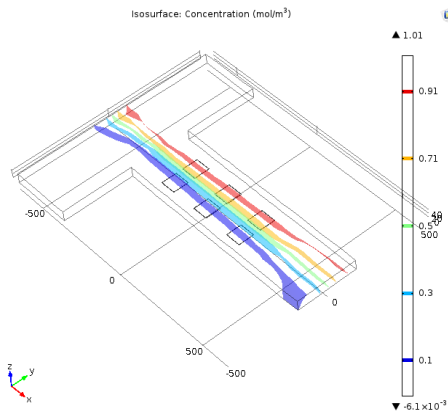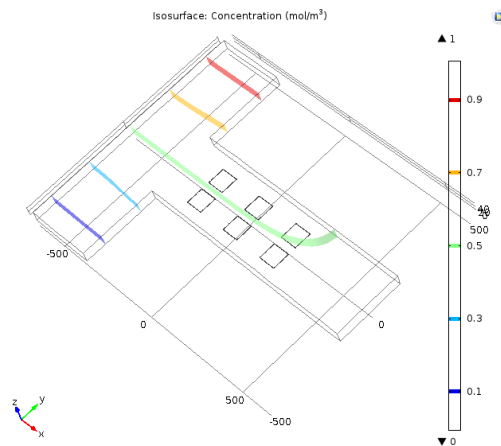

Figure 4.72 Representation of the 3D T-shaped microchannel with isosurface concentration having eight zeta potential patch of electric potential 50mV, -50mV, 50mV, -50mV, 50mV, -50mV, 50mV and -50mV respectively.

Figure 4.71 Representation of the 3D T-shaped microchannel surface concentration with eight zeta potential patch of electric potential 50mV, -50mV, 50mV, -50mV, 50mV, -50mV, 50mV and -50mV respectively.
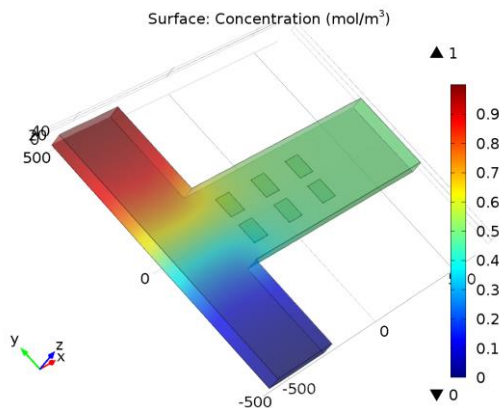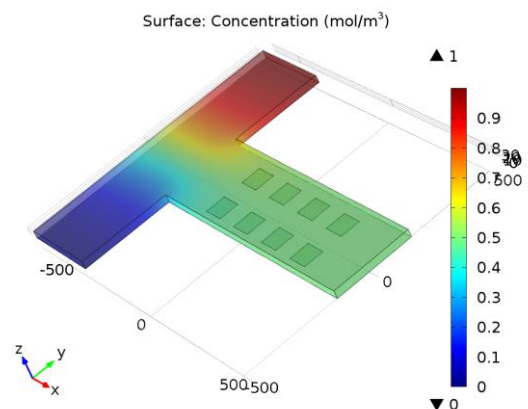

Figure 4.73 Representation of the 3D T-shaped microchannel surface concentration with eight zeta potential patch of electric potential 100mV, -100mV, 100mV, -100mV, 100mV, -100mV, 100mV and -100mV respectively.

38
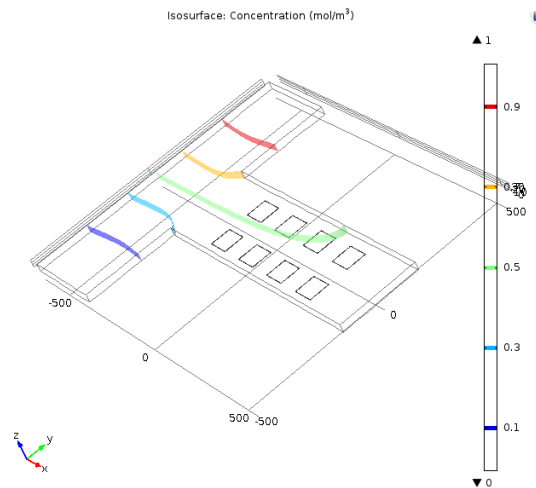
Figure 4.74 Representation of the 3D T-shaped microchannel with isosurface concentration having eight zeta potential patch of electric potential 100mV, -100mV, 100mV, -100mV, 100mV, -100mV, -100mV, 100mV and -100mV respectively.

3D Model C Inference:

In T-shaped 3D microfluidic micromixer with eight zeta potential patch of opposite electric potential, 25mV zeta potential solutions shows poor mixing efficiency, 50mV zeta potential solution shows slight increase whereas 100mV zeta potential exhibit complete mixing with 30 μm height micromixer for concentration 1 mol/m^3 and 0 mol/m^3 respectively. Hence, model C shows virtually no concentration mixing for 25mV zeta potential solution however slight concentration mixing with 50mV zeta potential and complete mixing efficiency within micromixer for 100mV zeta potential solution for two different concentration of 1 mol/m^3 and 0 mol/m^3 respectively.

4.2.4   3D Model D

T-shaped 3D micromixer with four long arm zeta potential patch of electric potential of 25mV, 50mV and 100mV respectively.
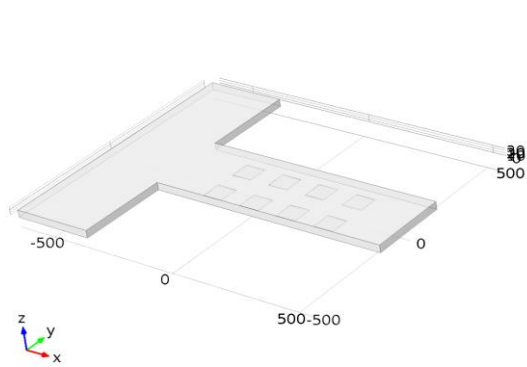
Multislice: Electric potential (V)
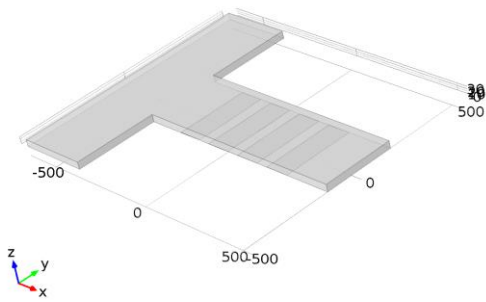
Figure 4.75 Representation of the 3D T-shaped microchannel with four long zeta potential patch placing.
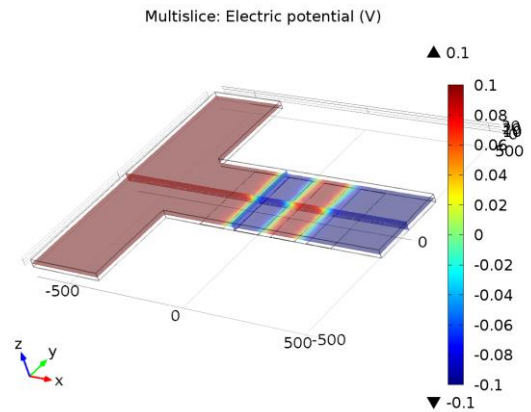
Figure 4.77 Representation of the 3D T-shaped microchannel with four long electric potential.
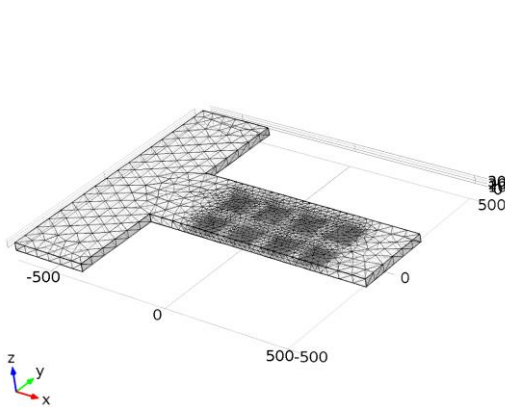

Surface: Concentration (mol/m³)
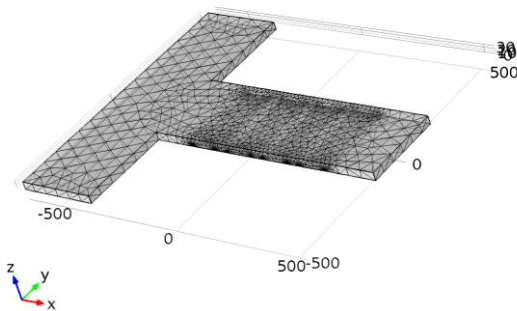
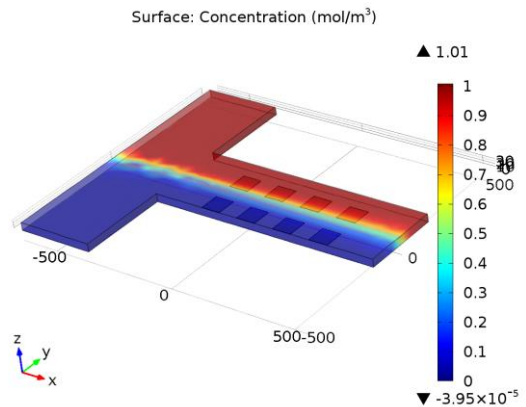**Figure 4.76 Representation of the 3D T-shaped microchannel meshing with four long zeta potential patch.**
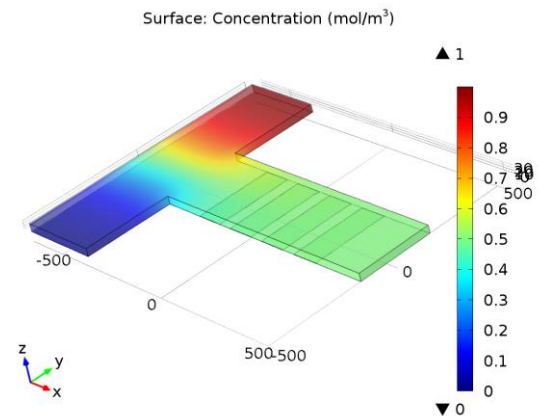
Figure 4.78 Representation of the 3D T-shaped microchannel surface concentration with four long zeta potential patch of electric potential 100mV, -100mV, 100mV and -100mV respectively.
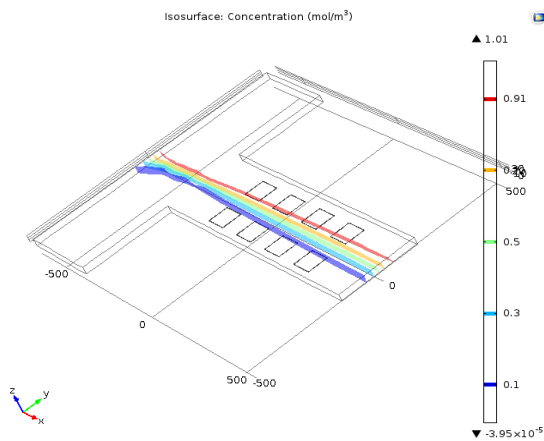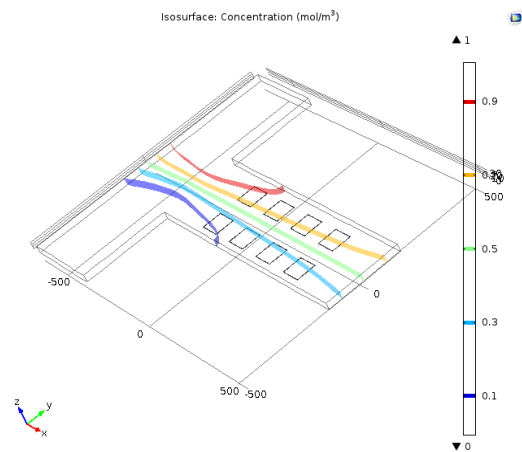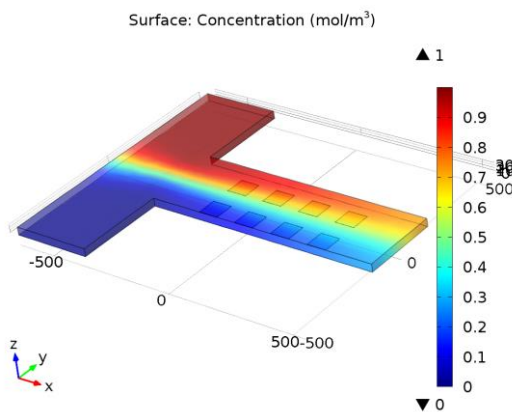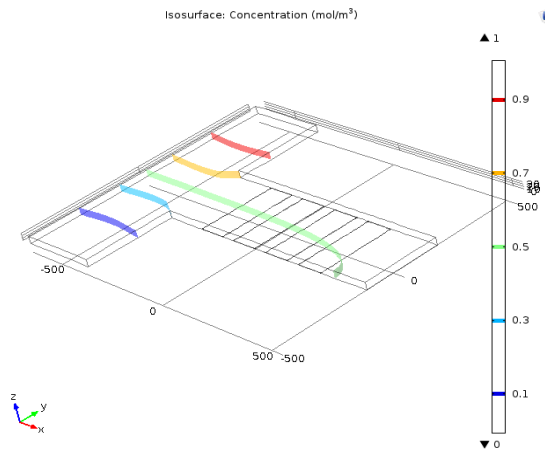
Figure 4.79 Representation of the 3D T-shaped microchannel with isosurface concentration having four long zeta potential patch of electric potential 100mV, -100mV, 100mV and -100mV respectively.

3D Model D Inference:

In T-shaped 3D microfluidic micromixer with four long arm zeta potential patch of opposite electric potential, 100mV zeta potential exhibit complete mixing with 30 μm micromixer height. Hence, model D shows complete mixing efficiency within micromixer for 100mV zeta potential solution for two different concentration of 1 mol/m^3 and 0 mol/m^3 respectively.

Chapter 5

Conclusion and future work

This thesis presents a modeling of electrokinetic mixing using electro-osmotic stationary and time-dependent micropumps via alternate zeta potential patches on the lower surface of the mixing chamber in lab on chip microfluidic device. Electro-osmotic flow is augmented using different model designs with alternate zeta potential values such as 25mV, 50mV and 100mV respectively to achieve high mixing efficiency in electrokinetically driven microfluidic system. 2D and 3D simulation electric contours and concentration gradients are derived by employing a Navier-Stokes for incompressible flow, convection-diffusion equation and Helmholtz-Smoluchowski slip velocity as appropriate boundary conditions.

Mixing efficiency in electrokinetically driven microfluidic system depends on number of patch, orientation and, mainly, higher magnitude of zeta potential. In general, simulations results indicate that the chaotic electrokinetic mixing increase with the increase in zeta potential values within the T-shaped micromixer, highest with zeta potential of 100mV for mixing for two different concentration of 1 mol/m^3 and 0 mol/m^3 respectively.

2D Simulations

There is a cumulative increase in mixing efficiency within T-shaped micromixer from 25mV up to 100mV for two different concentration of 1 mol/m^3 and 0 mol/m^3 respectively. Low concentration mixing is exhibit at 25mV zeta potential whereas 100mV zeta potential exhibit highest mixing.

3D Simulations

For zeta potential patch of four and six, 25mV and 50mV zeta potential shows constant and low mixing whereas with eight zeta potential patch, 25mV shows still low mixing but increase in 50mV mixing efficiency. Highest mixing efficiency is achieved using 100mV zeta potential in any zeta potential patch number and irrespective of their orientations for mixing for two different concentration of 1 mol/m^3 and 0 mol/m^3 respectively.

Therefore, 2D and 3D simulation models shows different mixing pattern for concentration mixing of 1 mol/m^3 and 0 mol/m^3 respectively.

Future work can be aimed to fabricate the microfluidic devices using various fabrication techniques such as laser ablation, optical lithography or microfabrication with photolithography. Fabrication workflow involves designated steps such as wafer cleansing, coating with photoresist, exposure to light, PDMS molding and bonding, etc. The geometry, number of patch and their orientation have to be taken into consideration when designing a microchip. The fabricated microchips can be employed to determine cell viability between different biological components (RBCs, WBCs, etc.), contact efficiency employing different lysing agent (SLS or NH4Cl), cytosol composition, mixing efficiency, etc.

References

[1] C. C. Chang and R. J. Yang. Electrokinetic mixing in microfluidic systems. Microfluid Nanofluid 3, (2007) 501–525.

[2] S. Wall. The history of electrokinetic phenomena. Current Opinion in Colloid and Interface Science 15, (2010) 119–124.

[3] C. C. Chang and R. J. Yang. Computational analysis of electrokinetically driven flow mixing with patterned blocks. J Micromech Microeng 14, (2004) 550–558.

[4] D. Li. Electrokinetics in microfluidics. Elsevier Academic Press 1, (2004).

[5] A. Ramos, H. Morgan, N. G. Green and A. Castellanos. AC electric field-induced fluid flow in microelectrodes. J Colloid Interf Sci 217, (1999) 420–422.

[6] I. Glasgow, J. Batton and N. Aubry. Electroosmotic mixing in microchannels. Lab on a Chip 6, (2004) 558–562.

[7] P. B. Howell, D. R. Mott, S. Fertig, C. R. Kaplan, J. P. Golden, E. S. Oran and F. S. Ligler. A microfluidic mixer with grooves placed on the top and bottom of the channel. Lab Chip 5, (2005) 524.

[8] A. Bandopadhyay, D. DasGupta, S. K. Mitra and S. Chakraborty. Electro-osmotic flows through topographically complicated porous media: Role of electropermeability tensor. Phys. Rev. E, (2013) 87.

[9] C. K. Chen and C. C. Cho. Electrokinetically driven flow mixing utilizing chaotic electric fields. Microfluid Nanofluid 5, (2008) 785.

[10] F. R. Phelan, P. Kutty and J. A. Pathak. An electrokinetic mixer driven by oscillatory cross flow. Microfluid Nanofluid 5, (2008) 101.

[11] H. Sugioka. Chaotic mixer using electro-osmosis at finite Péclet number. Phys. Rev. E, (2010) 81.

[12] S. Jeong, J. Park, J. M. Kim and S. Park. Microfluidic mixing using periodically induced secondary potential in electroosmotic flow. Journal of Electrostatics, 2011, 69, 429.

[13] C. C. Chang and R. J. Yang. Electroosmosis – a Mechanism of Micromixer and Micropump. J Micromech Microeng 14, (2004) 550.

[14] J. Lee, H. Moon, J. Fowler, T. Schoellhammer and C. J. Kim. Electrowetting and electrowetting-on-dielectric for microscale liquid handling. Sens Actuators A 95, (2002) 259–268.

[15] G. M. Whitesides. The origins and the future of microfluidics. Nature 442, (2006) 368–373.

[16] D. Mark, S. Haeberle, G. Roth, F. Stettenz and R. Zengerle. Microfluidic lab-on-a-chip platforms: requirements, characteristics and applications. Chem. Soc. Rev. 39, 2010 1153–1182.

[17] A. Manz, N. Graber and H. M. Widmer. Miniaturized total chemical analysis systems: a novel concept for chemical sensing. Sens. Actuators B Chem.1, (1990) 244–248.

[18] D. Janasek, J. Franzke and A. Manz. Scaling and the design of miniaturized chemical-analysis systems. Nature 442, (2006) 374–380.

[19] J. K. Chen, W. J. Luo and R. J. Yang. Electroosmotic flow driven by DC and AC electric fields in curved microchannels. Jap J Appl Phys 45, (2006) 7983–7990.

[20] D. Erickson and D. Li. Influence of Surface Heterogeneity on Electrokinetically Driven Microfluidic Mixing. Langmuir 18, (2002) 1883-1892.

[21] R. F. Ismagilov, A. D. Stroock, P. A. Kenis, G. M. Whitesides and H. A. Stone. Experimental and theoretical scaling laws for transverse diffusive broadening in two-phase laminar flow in microchannels. Appl Phys Lett 76, (2000) 2376–2378.

[22] S. Wiggins, J. M. Ottino. Foundations of chaotic mixing. Phil Trans R Soc Lond A 362, (2004) 937–970.

[23] J. M. Ottino. The kinematics of mixing: stretching, chaos, and transport. Cambridge University Press, Cambridge, (1989).

[24] R. J. Hunter. Zeta potential in colloid science: principles and applications. Academic Press, New York, (1981).

[25] L. M. Fu, R. J. Yang, C. H. Lin and Y. S. Chien. A novel microfluidic mixer utilizing electrokinetic driving forces under low switching frequency. Electrophoresis 5, (2005) 1814–1824.

[26] Y. Wang, J. Zhe, P. Dutta and B. Chung. A Microfluidic Mixer Utilizing Electrokinetic Relay Switching and Asymmetric Flow Geometries. J. Fluids Engineering 129, (2007) 395-403.

[27] S. M. Kim, M. A. Burns and E. F. Hasselbrink. Electrokinetic Protein Preconcentration Using a Simple Glass/Poly(dimethylsiloxane) Microfluidic Chip. Anal. Chem. 78, (2006) 4779-4785.

[28] K. Anwar, T. Han, S. Yu and S. M. Kim. An Integrated Micro-Nanofluidic System for Sample Preparation and Preconcentration of Proteins. Microchimica Acta 173 (3), (2011) 331-335.

[29] J. T. Coleman, J. Mckechnie and D. Sinton. High-efficiency electrokinetic micromixing through symmetric sequential injection and expansion. Lab Chip 6, (2006) 1033–1039.

[30] Y. T. Zhang, H. Chen, I. Mezic, C. D. Meinhart, L. Petzold and N. C. MacDonald. SOI Processing of a Ring Electrokinetic Chaotic Micromixer. Nanotechnology Conference and Trade Show 1, (2004) 292–295.

[31] T. Dong, M. Molino and D. Demarchi. Cell-based Digital Microfluidic Chip for Drug Mixing and Droplets Generation: Design and Simulation. 5th International Conference on BioMedical Engineering and Informatics, (2012).

[32] G. H. Tanga, L. Zhuo, J. K. Wang, Y. L. He and W. Q. Tao. Electroosmotic flow and mixing in microchannels with the lattice Boltzmann method. J. Appl. Phys. 100, (2006) 094908.

[33] H. S. Seo, B. Han and Y. J. Kim. Numerical Study on the Mixing Performance of a Ring-Type Electroosmotic Micromixer with Different Obstacle Configurations. J. Nanosci. Nanotechnol. 12, (2012) 4523–4530.